



# Design, synthesis, and biological evaluation of 2,4-diamino pyrimidine derivatives as potent FAK inhibitors with anti-cancer and anti-angiogenesis activities



Shan Wang<sup>a, c, 1</sup>, Rong-Hong Zhang<sup>a, b, 1</sup>, Hong Zhang<sup>c</sup>, Yu-Chan Wang<sup>c</sup>, Dan Yang<sup>c</sup>, Yong-Long Zhao<sup>c</sup>, Guo-Yi Yan<sup>d</sup>, Guo-Bo Xu<sup>c</sup>, Huan-Yu Guan<sup>c</sup>, Yan-Hua Zhou<sup>b</sup>, Dong-Bing Cui<sup>b</sup>, Ting Liu<sup>a, c</sup>, Yong-Jun Li<sup>a, c</sup>, Shang-Gao Liao<sup>c, \*\*, \*</sup>, Meng Zhou<sup>a, c, \*</sup>

<sup>a</sup> State Key Laboratory of Functions and Applications of Medicinal Plants, Engineering Research Center for the Development and Application of Ethnic Medicine and TCM (Ministry of Education), Guizhou Medical University, Guiyang, 550004, PR China

<sup>b</sup> Center for Tissue Engineering and Stem Cell Research, Key Laboratory of Regenerative Medicine of Guizhou Province, Guizhou Medical University, Guiyang, 550004, PR China

<sup>c</sup> School of Pharmacy, Guizhou Medical University, Gui'an New District, Guizhou, PR China

<sup>d</sup> Department of Hepatobiliary Pancreatic Surgery, Henan Provincial People's Hospital, Henan University, Zhengzhou, PR China

## ARTICLE INFO

### Article history:

Received 19 January 2021

Received in revised form

15 May 2021

Accepted 20 May 2021

Available online 29 May 2021

### Keywords:

FAK inhibitor

DAPY

Antitumor

Anti-angiogenesis

Structure-activity relationship

## ABSTRACT

A series of 2,4-diamino pyrimidine (DAPY) derivatives were designed, synthesized, and evaluated as inhibitors of focal adhesion kinase (FAK) with antitumor and anti-angiogenesis activities. Most compounds effectively suppressed the enzymatic activities of FAK, and the IC<sub>50</sub>s of **11b** and **12f** were 2.75 and 1.87 nM, respectively. **11b** and **12f** exhibited strong antiproliferative effects against seven human cancer cells, with IC<sub>50</sub> values against two FAK-overexpressing pancreatic cancer cells (PANC-1 and BxPC-3) of 0.98 μM, 0.55 μM, and 0.11 μM, 0.15 μM, respectively. Moreover, **11b** and **12f** obviously suppressed the colony formation, migration, and invasion of PANC-1 cells in a dose-dependent manner. Meanwhile, these two compounds could induce the apoptosis of PANC-1 cells and arrest the cell cycle in G2/M phase according to the flow cytometry assay. Western blot revealed that **11b** and **12f** effectively inhibited the FAK/PI3K/Akt signal pathway and significantly decreased the expression of cyclin D1 and Bcl-2. In addition, compounds **11b** and **12f** potently inhibited the antiproliferative of HUVECs and obviously altered the cell morphology. **11b** and **12f** also significantly inhibited the migration, tube formation of HUVECs and severely impaired the angiogenesis in the zebrafish model. Overall, these results revealed the potential of compounds **11b** and **12f** as promising candidates for further preclinical studies.

© 2021 Elsevier Masson SAS. All rights reserved.

## 1. Introduction

Focal adhesion kinase (FAK), which locates at the sites of focal adhesions, is a non-receptor tyrosine protein kinase [1], regulating multiple signal pathways in the adhesion, proliferation, migration,

invasion and angiogenesis of cancer cells [2]. Numerous reports demonstrated that FAK was overexpressed in a variety of cancer cells [3], including prostate, lung, breast, cervical and kidney cancer cells [4–7], and inhibition the overexpression of FAK significantly suppresses the progression of cancer, and FAK is therefore considered a promising target for cancer treatment [8]. Up to present, numbers of FAK inhibitors have been developed, and some have entered preclinical or clinical trials as anticancer agents, including PF-573228 (**1**, Fig. 1), PF-562271 (**2**), and CEP-374220 (**3**) [9–12]. To improve the selectivity of kinase inhibition, the hinge-binders PND1186 (**4**) [13,14] and Compound 32 (**5**) [15] were discovered with effective FAK inhibitory activities, and allosteric inhibitors Compound 1 (**6**) was reported targeting the allosteric site outside of the adenosine triphosphate (ATP)-binding site [16]. Defactinib (**7**),

\* Corresponding author. State Key Laboratory of Functions and Applications of Medicinal Plants, Engineering Research Center for the Development and Application of Ethnic Medicine and TCM (Ministry of Education), Guizhou Medical University, Guiyang, 550004, PR China.

\*\* Corresponding author.

E-mail addresses: [lishang@163.com](mailto:lishang@163.com) (S.-G. Liao), [gmu\\_mengzhou@163.com](mailto:gmu_mengzhou@163.com) (M. Zhou).

<sup>1</sup> These authors contributed equally to this work.

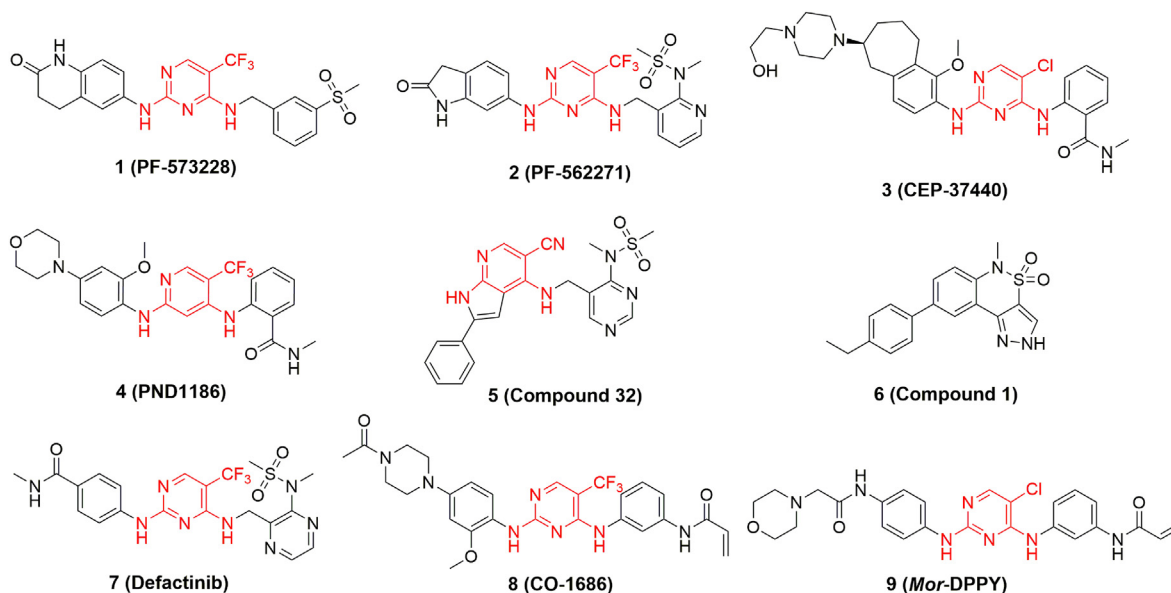


Fig. 1. Chemical structures of potent FAK (1–7) and EGFR (8, 9) inhibitors with 2,4-diamino pyrimidine (DAPY) fragment.

also known as PF-04554878 and VS-6063, is an orally effective ATP competitive product and is now in the phase II clinical trial. This inhibitor was reported to prevent the integrin-mediated activation of several downstream signal transduction pathways, including RAS/MEK/ERK and PI3K/Akt, thus inhibiting the migration, proliferation, survival and angiogenesis of cancer cells [17]. Therefore, searching for effective FAK inhibitor offers new strategy for cancer therapy.

2,4-Diamino pyrimidine (DAPY) is a useful fragment in the design of anticancer agents [18], and many promising FAK inhibitors contains this fragment (e.g., 1–4 in Fig. 1). Moreover, some DAPY derivatives, like CO-1686 (8, Phase III) [19] and Mor-DAPY (9) [20], were demonstrated to possess obvious anti-angiogenesis activities. Further investigation showed that the pyrimidine core of DAPY anchored to the hinge region of FAK through forming two hydrogen bonds with Cys 502 (Fig. 2) [21], and two aryl residue A

and B stretched toward the solvent region and the DFG motif of the activation loop, respectively [22]. Recent research revealed that the hydrophobic interaction of aryl residue B with the DFG-helical region in FAK improved the selectivity of FAK inhibitors, making residue B a key substructure for the optimization of DAPY inhibitors [23]. Different structures have been introduced to residue B in DAPY-type FAK inhibitors, however, no systematic structure-activity relationship related to this substructure has been reported. To optimize the structure of residue B and its distance to the pyrimidine core, a variety of substituents were introduced to the aryl residue B, and a carbon-elongation of the distance between the pyrimidine and residue B was also investigated in this study (Fig. 2). The structure-activity relationship was then discussed. The anticancer and anti-angiogenesis activities of the designed compounds were further evaluated *in vitro* and *in vivo*. The results showed that, most of these compounds not only displayed strong anti-FAK

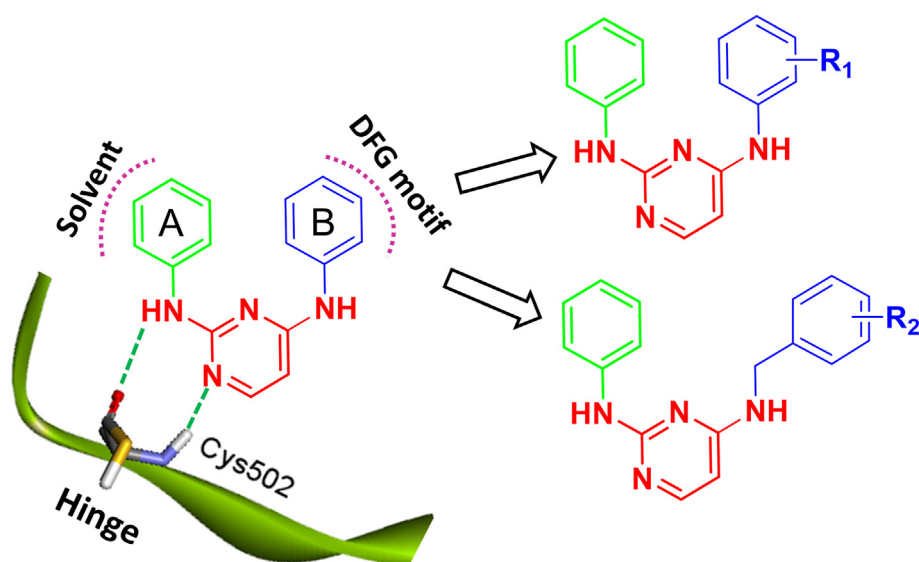


Fig. 2. Designed strategy of target compounds.

activity, but also displayed pronounced anticancer activity and high angiogenesis inhibitory effect.

## 2. Results and discussion

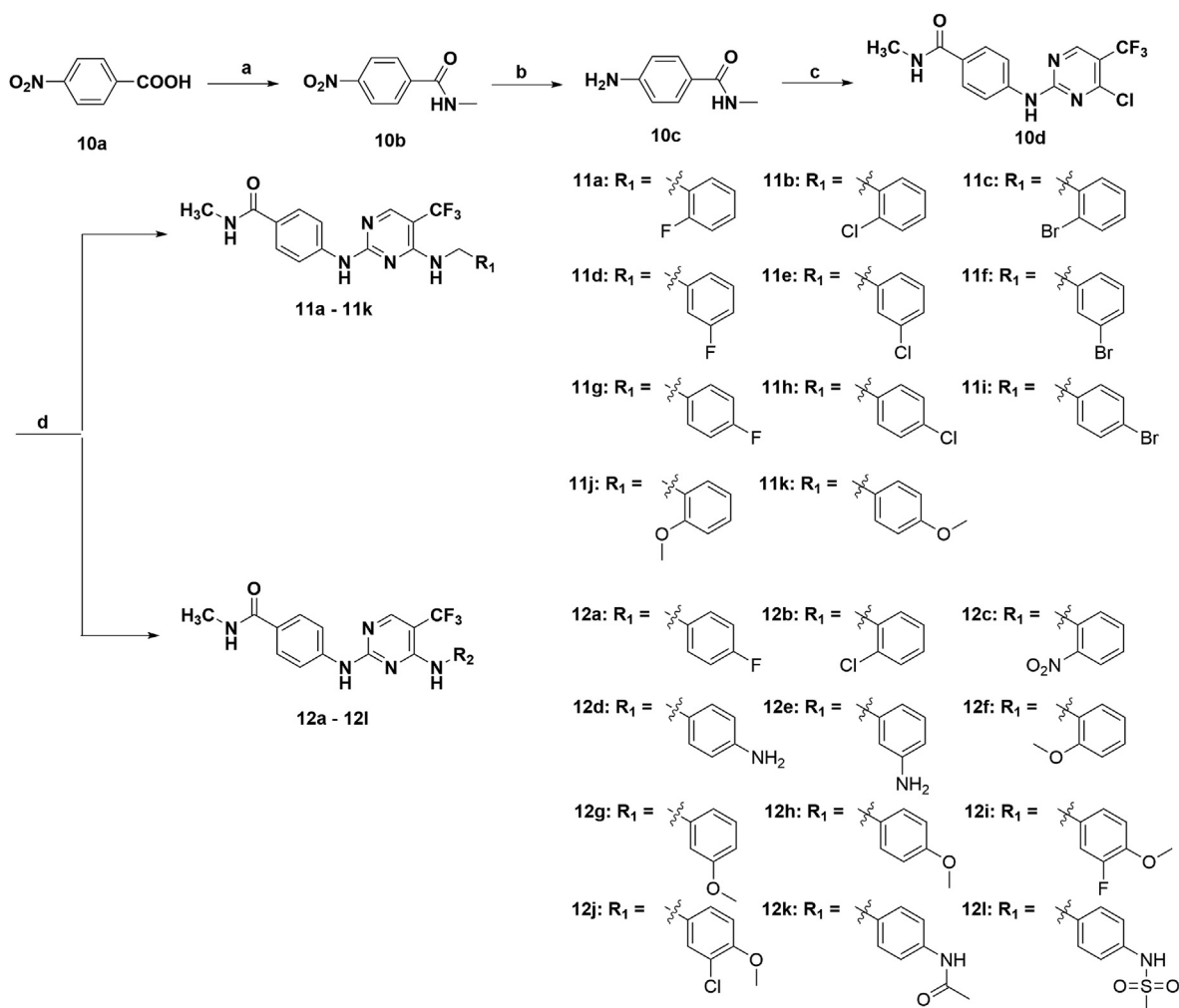
### 2.1. Chemistry

Synthesis of the DAPY derivatives (**11a-11k**, **12a-12l**) were depicted in Scheme 1. Commercially available 4-nitrobenzoic acid (**10a**) was refluxed in oxalyl chloride to give the reactive acid chloride intermediate, which was converted to *N*-methyl-4-nitrobenzamide (**10b**) under basic conditions (Et<sub>3</sub>N). The nitro group of compound **10b** was reduced by the stannous chloride to give the 4-amino-*N*-methylbenzamide (**10c**). Compound **10c** was added to a solution of 2,4-dichloro-5-(trifluoromethyl)pyrimidine in DCM/*t*-BuOH (1:1) with the presence of zinc bromide and Et<sub>3</sub>N to afford the key intermediate **10d**. Ultimately, the target compounds **11a-11k** were conveniently synthesized *via* the coupling reaction of compound **10** with substituted benzylamines in the presence of *N,N*-diisopropylethylamine (DIEA). Compounds **12a-12l** were prepared using similar reaction conditions as depicted in Scheme 1, and the substituted benzylamine in the last step were replaced by substituted anilines.

### 2.2. Anti-cancer activity

#### 2.2.1. *In vitro* activity against FAK kinase and analysis of the structure-activity relationship

All the synthesized compounds (**11a-11k** and **12a-12l**) were evaluated for the FAK enzyme inhibitory activity using homogeneous time-resolved fluorescence (HTRF) assays, and defactinib was tested for comparison. Results revealed that defactinib strongly inhibited the activity of FAK with IC<sub>50</sub> of 1.16 nM (inhibitory concentration of 50%, Table 1), which was close to the reported data [24]. Clearly, the newly synthesized compounds exhibited effective inhibitory activities with IC<sub>50</sub> ranging from 1.87 to 55.63 nM except compound **12g** (IC<sub>50</sub> = 2321 nM). For benzylamine derivatives **11a-11k** that carry a methylene between pyrimidine and residue B, introduction of halogens (F, Cl, Br) to the *ortho* or *meta* position of the benzyl group (**11a-11f**) basically retained the enzyme inhibitory activities. In particular, inclusion of a chlorine atom in C1 (**11b**) exhibited the strongest FAK inhibition (IC<sub>50</sub> = 2.75 nM). Whereas, introduction of halogens at *para* position (**11g-11i**) obviously impaired the inhibitory effect. The hydrophobic methoxy group was then evaluated. Similarly, compound **11j** with a hydrophobic methoxy group at *ortho* position also displayed an excellent inhibitory activity (IC<sub>50</sub> = 5.73 nM), whereas the FAK enzyme inhibitory effect was reduced five folds when the hydrophobic



**Scheme 1.** Synthetic route of title compounds **11a-11k** and **12a-12l**. Reagents and conditions: (a) i: (COCl)<sub>2</sub>, reflux, 3 h; ii: CH<sub>3</sub>NH<sub>2</sub>, Et<sub>3</sub>N, DCM, 68 °C, 3 h, 57%; (b) SnCl<sub>2</sub>·2H<sub>2</sub>O, EtOAc, 80 °C, 3 h, 75%; (c) 2,4-Dichloro-5-(trifluoromethyl)pyrimidine, ZnBr<sub>2</sub>, Et<sub>3</sub>N, DCM/*t*-BuOH (1:1), 0 °C, 20 h, 51%; (d) DIEA, CH<sub>3</sub>CN, 90 °C, 6–12 h, 18–65%.

**Table 1**  
Kinase inhibitory activities and antiproliferative activities of all target compounds against different human cell lines.

Compound	Enzymatic activity (IC <sub>50</sub> , nM) <sup>a</sup>		Antiproliferative activity (IC <sub>50</sub> /μM) <sup>b</sup>									
	FAK	VRGFR2	Cancer cells								Normal cells	
			PANC-1	BxPC-3	MCF-7	MDA-MB-231	HepG2	A549	HCT-15	HUVEC	HEK293	L02
<b>11a</b>	5.80	– <sup>c</sup>	7.18	12.49	6.92	3.37	0.64	4.29	7.86	>20	>20	3.22
<b>11b</b>	2.75	146.8	0.98	0.55	1.47	0.76	0.71	2.72	0.79	2.29	4.92	15.14
<b>11c</b>	6.29	–	3.68	0.58	1.50	1.58	0.93	3.86	0.94	4.53	1.96	8.04
<b>11d</b>	4.24	–	5.46	6.48	4.77	1.96	6.81	7.16	>20	>20	>20	9.78
<b>11e</b>	5.71	–	2.36	4.98	3.56	6.27	3.65	3.56	3.16	2.72	6.78	15.62
<b>11f</b>	4.02	–	3.41	3.29	3.54	8.34	3.46	3.69	3.79	6.95	5.49	12.39
<b>11g</b>	4.44	–	3.15	3.59	5.69	1.68	2.97	3.31	4.18	3.22	3.89	17.35
<b>11h</b>	35.33	–	4.84	5.07	7.10	4.56	1.97	4.10	3.65	5.55	17.73	>20
<b>11i</b>	39.66	–	4.72	4.36	12.31	5.05	2.79	4.20	5.03	>20	>20	>20
<b>11j</b>	5.73	–	2.09	1.82	>20	2.56	0.31	1.30	7.04	>20	>20	18.93
<b>11k</b>	28.73	–	2.33	2.57	4.42	4.45	0.89	2.37	5.84	5.47	>20	8.94
<b>12a</b>	31.25	–	0.18	0.32	8.54	3.55	0.25	0.81	4.24	1.32	>20	2.69
<b>12b</b>	34.37	–	0.85	1.68	0.84	0.93	0.57	1.18	0.70	0.71	1.53	>20
<b>12c</b>	11.69	–	2.81	1.47	1.37	2.58	0.64	2.11	1.71	1.02	2.75	15.84
<b>12d</b>	24.19	–	0.99	0.92	6.80	0.39	3.89	8.36	1.25	1.13	7.93	4.04
<b>12e</b>	30.77	–	6.05	0.45	2.26	1.16	0.45	3.53	1.37	0.70	1.27	4.93
<b>12f</b>	1.87	291.8	0.11	0.15	0.25	0.35	0.14	0.65	0.12	0.18	16.17	>20
<b>12g</b>	2321	–	>20	>20	>20	>20	>20	>20	>20	>20	>20	>20
<b>12h</b>	55.63	–	1.72	0.38	1.59	0.52	0.63	1.99	1.25	1.00	0.79	4.62
<b>12i</b>	39.07	–	4.79	1.59	3.88	0.93	0.62	2.60	4.17	1.67	6.73	5.48
<b>12j</b>	34.74	–	3.97	1.57	>20	2.88	1.25	3.60	3.39	>20	>20	>20
<b>12k</b>	21.22	–	5.25	1.10	5.41	5.87	0.51	5.37	2.23	>20	8.96	3.13
<b>12l</b>	18.19	–	6.64	1.52	11.96	8.64	0.56	5.75	8.13	>20	12.43	16.98
<b>Defactinib</b>	1.16	273.2	3.48	3.25	5.81	3.75	3.69	4.09	4.36	3.24	4.07	4.66

<sup>a</sup> The IC<sub>50</sub> values are presented as the mean (nM) values from three separate experiments.

<sup>b</sup> Concentration that inhibits the proliferation of cancer cells by 50%. IC<sub>50</sub> values are average for at least three independent experiments.

<sup>c</sup> Not test.

methoxy group migrated to *para* position (**11k**).

On the other hand, for aniline derivatives, more substituents were investigated. As shown in Table 1, introduction of Cl (**12a**) and F (**12b**) to the *ortho* and *para* positions of the phenyl group both exhibited good activities, with IC<sub>50</sub> values of 31.25 and 34.37 nM, respectively. The enzyme inhibitory effect increased nearly three folds with the addition of an electron-withdrawing nitro group at *ortho* at position (**12c**), and the IC<sub>50</sub> improved slightly by the introduction of electron-donating amino group to *meta* (**12d**) and *para* (**12e**) positions. Interestingly, the inclusion of a methoxyl group in the *ortho* (**12f**), *meta* (**12g**), and *para* (**12h**) positions of the phenyl group exhibited quite different activities. Aniline derivatives **12f** with a methoxyl group at the *ortho* position significantly inhibited the FAK activity with IC<sub>50</sub> of 1.87 nM. By contrast, the activity was markedly decreased when the methoxyl group was migrated to the *meta* (**12g**) or *para* (**12h**) position, with IC<sub>50</sub> values of 2321 and 55.63 nM, respectively. Based on the above observations, two compounds (**12i**, **12j**) with a *para*-methoxyl group and a *meta*-halogen atom were synthesized, yet no satisfactory activity was achieved, which suggested that the cooccurrence of both substituents was detrimental to the activity. In addition, compounds with larger-size substituents (**12k** and **12l**) at the *para* position were also evaluated, and only partial inhibitory activities were kept compared with **12f**. Therefore, it can be concluded that substituents introduced to the *ortho* position is more tolerant than to the *meta* and *para* positions, and a hydrophobic group is more desired for FAK inhibitory activity.

### 2.2.2. Antiproliferative activity

The title compounds were then evaluated for the antiproliferative activity towards human cancer cells by using the MTT assay. Two FAK-overexpressed pancreatic cancer cells (BxPC-3 and PANC-1), two breast cancer cells (MCF-7 and MDA-MB-231), liver cancer cell (HepG2), lung cancer cell (A549), and human colon cancer cell (HCT-15) were selected to test their toxicities.

Meanwhile, human umbilical vein endothelial cell (HUVEC) was used to investigate anti-angiogenesis activity of the target molecules. Defactinib was evaluated as a reference. Results showed that most of the compounds except **12g** intensively inhibited the cancer cell lines with IC<sub>50</sub> values comparable to or lower than that of defactinib (Table 1). The newly synthesized compounds showed remarkable antiproliferative effect against FAK-overexpressed BxPC-3 and PANC-1 cells, with IC<sub>50</sub> values ranging from 0.11 to 7.18 μM. These analogues also effectively inhibited the proliferation of metastatic cancer cells (MCF-7, MDA-MB-231, HepG2, A549, and HCT-15). Particularly, 14 compounds displayed significant antiproliferative effect against HepG2 with IC<sub>50</sub> values lower than 1 μM (Table 1). Similar to the kinase inhibitory effects observed for the synthesized compounds, **11b** and **12f** seemed to be the most active compounds toward most of the seven human cancer cells, with IC<sub>50</sub>s less than 2.72 and 0.65 μM, respectively, and were more potent than the positive control defactinib. Interestingly, the morphology of cancer cells was changed obviously when treating with different concentrations of **11b** and **12f**, and the cells were extremely swollen, indicating disorganization of the internal architecture (Supporting Information Fig. S1-S6).

To evaluate the safety of the target compounds, the toxicity against human embryonic kidney cells HEK293 and hepatic cells L02 were test as well (Table 1). Compared with the antiproliferative effect against cancer cells, the synthesized compounds displayed a lower toxicity to normal cells. Among them, the IC<sub>50</sub> values of **12f** were 16.17 and > 20 μM against HEK293 and L02 cells respectively, indicating considerable safety. Since **11b** and **12f** possess significant antiproliferative potency, both compounds were further investigated for their anti-cancer effect against PANC-1 cell lines.

### 2.2.3. Colony formation assay

To better understand the anti-cancer activity of **11b** and **12f**, colony formation assay was used to evaluate their antiproliferative effects against PANC-1 cells. The cells were treated with **11b** and **12f**

at concentrations of 0.125, 0.25, 0.5, 1, 2  $\mu\text{M}$  for 10 days. As shown in Fig. 3A, **11b** and **12f** obviously suppressed the colony formation of PANC-1 cells, which were more potent than defactinib at 1 and 2  $\mu\text{M}$  ( $p < 0.001$ , Fig. 3B). Very few colonies were observed in plates after treated with compound **12f** at the concentrations higher than 0.5  $\mu\text{M}$  ( $p < 0.001$ ). For the other FAK-overexpressed BxPC-3 cells, **11b** and **12f** exhibited stronger antiproliferation activity than in PANC-1 cells, and 0.5  $\mu\text{M}$  of **12f** and 2  $\mu\text{M}$  of **11b** completely eliminated the colony formation (Supporting Information Fig. S8). Similar colony formation inhibitory effects (better than those of defactinib) were also observed for both compounds toward MCF-7, MDA-MB-231, HepG2, and HCT-15 cells (Supporting Information Fig. S9-12), indicating strong antiproliferation effects.

#### 2.2.4. Migration assay

Cell scratch assay was performed to study the effect of compounds **11b** and **12f** on the migration of PANC-1 cells. The data shown in Fig. 4 revealed that the scratched area in the control group was almost covered after 24 h (Fig. 4A), with a mobility of approximately 90% (Fig. 4B). By contrast, the cells treated with **11b** and **12f** exhibited slower recovery of the scratched areas in a concentration-dependent manner. The migration rates of **11b** and **12f** were much lower than defactinib at all concentrations ( $p < 0.01$ ). In particular, at 8  $\mu\text{M}$ , the migration rates of compounds **11b** and **12f** were only 10.43% and 16.36%, respectively.

#### 2.2.5. Invasion assay

Cell invasion is an important malignant behavior during the metastasis of cancer [25], and the invasion inhibitory activities of **11b** and **12f** were analyzed using transwell assay. Results revealed that, compared with defactinib, compounds **11b** and **12f** significantly inhibited the invasion of PANC-1 cells at all tested concentrations (1, 2, 4  $\mu\text{M}$ ,  $p < 0.001$ , Fig. 5A). In particular, almost no cancer cell was observed at 4  $\mu\text{M}$  for **11b** or 2  $\mu\text{M}$  for **12f** (Fig. 5B).

#### 2.2.6. Morphological analysis

In order to evaluate the effect of **11b** and **12f** to the morphological change of PANC-1 cells, the F-actin filaments were stained with Phalloidin-FITC and the nucleus was stained with DAPI. As illustrated in Fig. 6, cells in control group showed a regular array of F-actin filaments present along the cells that evenly radiated to the cell membrane from the nucleus. However, after treated with 0.25, 0.5, 1, 2, 4 and 8  $\mu\text{M}$  of **7b** and **7f** for 48 h, PANC-1 cells got swollen and the cells exhibited a reduced amount of F-actin and a disorganization of actin filaments. Microfilaments are the main part to maintain the normal architecture of cell and play an important role in the motility, differentiation division and membrane organization of cells [26]. Thus, the architecture of PANC-1 cell was damaged and the motility was severely impaired, leading to the inhibition of migration and invasion.

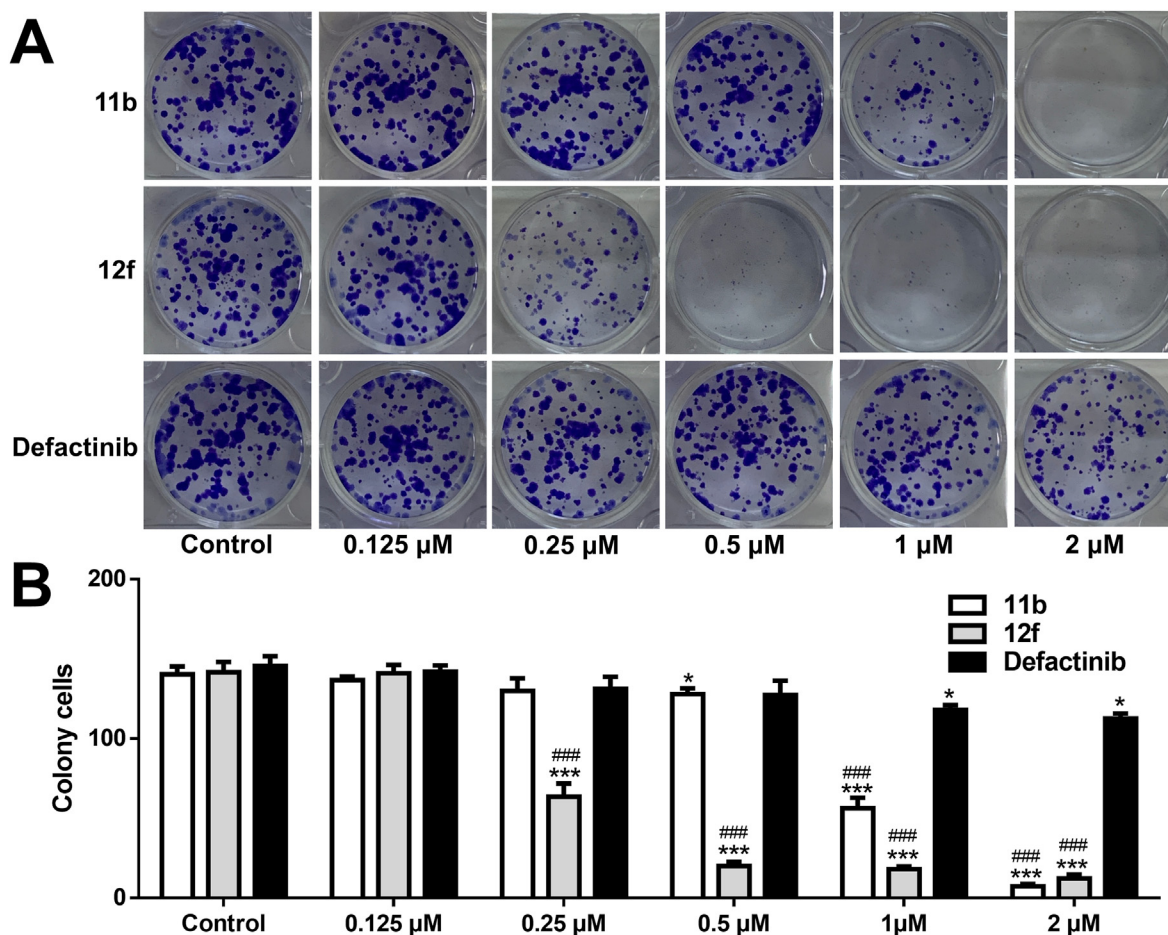


**Fig. 3.** Effects of **11b** and **12f** on the colony formation of PANC-1 cells. (A) PANC-1 cells were treated with various concentrations (0.125, 0.25, 0.5, 1, 2  $\mu\text{M}$ ) of **11b** and **12f** for 10 d, and the colonies were stained by crystal violet. (B) Quantifications of colony cells. Data were expressed as the mean  $\pm$  SD of three independent experiments. \*:  $p < 0.05$ , \*\*:  $p < 0.01$ , \*\*\*:  $p < 0.001$ , vs. control; ###:  $p < 0.001$ , vs. defactinib at the same concentration.

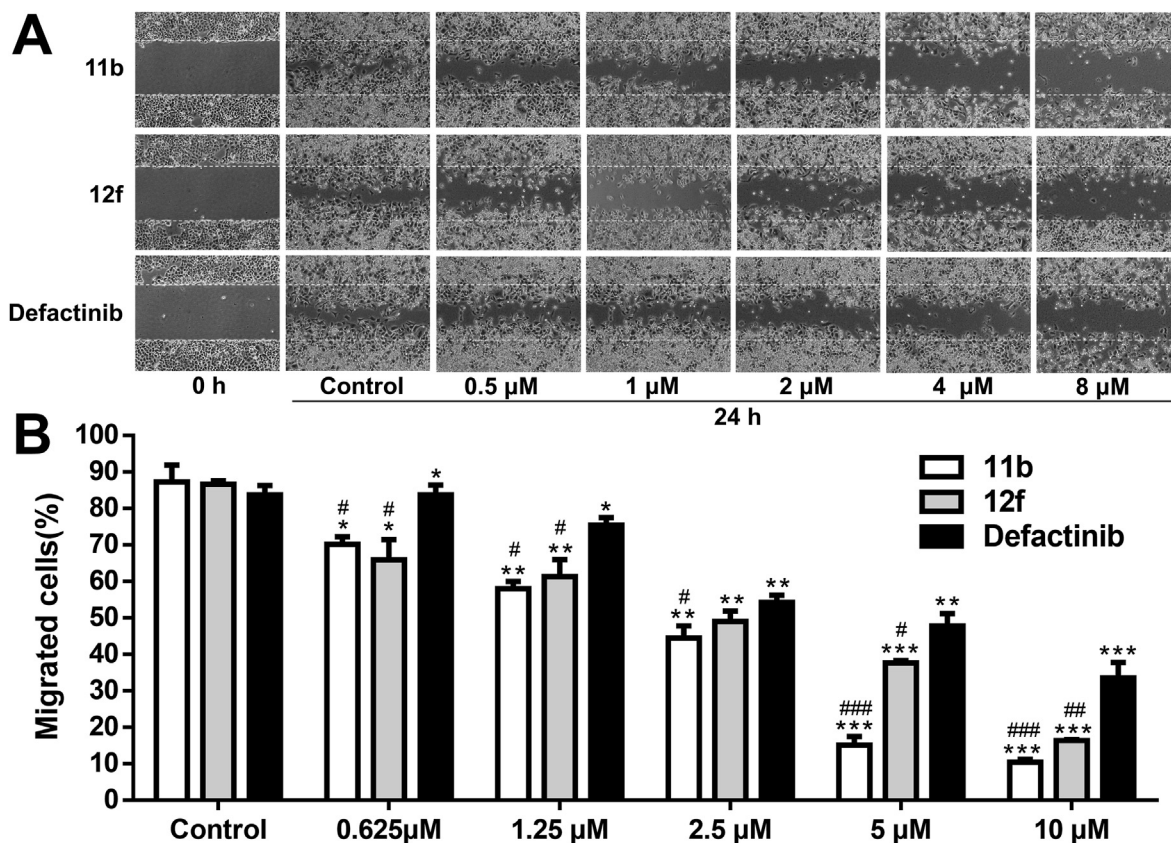


**Fig. 4.** Effects of compounds **11b** and **12f** on the migration of PANC-1 cells *in vitro* determined by scratch assay ( $\times 100$ ). (A) Images of PANC-1 cells migration inhibited by **11b** and **12f** ( $\times 40$ ). (B) Filled areas calculated by ImageJ software. \*:  $p < 0.05$ , \*\*:  $p < 0.01$ , \*\*\*:  $p < 0.001$  vs. control group; #:  $p < 0.05$ , ##:  $p < 0.01$ , ###:  $p < 0.001$ , vs. defactinib at the same concentration;  $n = 3$ .

### 2.2.7. Apoptosis analysis

Since the morphology changing of cancer cells was observed in the above experiment, propidium iodide (PI) staining was used to evaluate the effect of **11b** and **12f** on cancer cell apoptosis. After incubation of PANC-1, BxPC-3, HepG2 and HCT-15 cells with 0.1, 0.5 and 2.5  $\mu\text{M}$  of **11b** and **12f** for 48 h, fragmentation of chromatin indicating an early apoptosis were observed (Supporting Information Fig. S13-S16), and the apoptotic rates of compounds **11b** and **12f** were higher than that of defactinib. Then double staining with fluorescein diacetate (FDA)/PI was used to monitor the apoptosis induced by **11b** and **12f**. As shown in Fig. 7A, vital cells that took up the fluorogen FDA (green) were decreased and increased PI staining (red) were observed in dead cells with the concentration increasing, manifesting increased cell death relative to untreated control cells.

To better understand the characteristics of compounds **11b** and **12f** on the apoptosis, nuclear morphology was examined by microscopy using Hoechst 33258 staining (Fig. 7B). In the control group, the nuclei of PANC-1 cells were stained in blue and were uniform in shape. However, after adding of 0.25, 0.5, 1, 2, and 4  $\mu\text{M}$  of **11b** and **12f**, the morphology of PANC-1 cells altered significantly. Swollen chromatin was observed in the cancer cells treated with **11b** and **12f**, the chromatin was brighter than that in the control group. Nuclear fragmentation was also emerged, which were quite different from the morphological hallmark of typical apoptosis [27,28].

### 2.2.8. Flow cytometry assay

To evaluate the anti-cancer characteristics of compounds **11b** and **12f**, cell apoptosis and cycle were further analyzed by flow

cytometry analysis. As illustrated in Fig. 8, **11b** and **12f** indeed increased the apoptosis of PACN-1 cells in a concentration-dependent manner, with apoptotic rates of 2.31%, 10.30%, 12.02% for **11b** and 10.05%, 10.68%, 32.93% for **12f** at concentrations of 0.2, 1 and 5  $\mu\text{M}$ , respectively. Moreover, the cell cycle progression was significantly affected by **11b** and **12f** (Fig. 9). Compared with the control group, the percentage of cells in the G2/M phase increased from 13.2% to 54.2%, and for compound **12f**, the percentages increased to 78.0%. In contrast, cells in S and G0/G1 phase decreased concomitantly. Accordingly, compounds **11b** and **12f** induced the arrest of a significant percentage of cells in G2/M phase.

### 2.2.9. Western blot

Activation of the FAK/phosphatidylinositol 3-kinase (PI3K)/Akt signaling pathway has been correlated with the proliferation and metastasis of cancer cells [29,30], and thus the components of this pathway were evaluated by Western blot in PANC-1 cell lines. The level of FAK and its active phosphorylated form pFAK (Y397) were assessed, as well as the downstream members of the pathway: PI3K, Akt and their active forms pPI3K (Y458) and pAkt (S473) [31]. As depicted in Fig. 10A, the expression of FAK was maintained after the treatment of **11b**, whereas pFAK/FAK relative expression were significantly decreased with treating 0.5, 1, 2, and 4  $\mu\text{M}$  of **11b** ( $p < 0.01$ ), indicating that FAK-kinase activity was severely impaired. PI3K activity was decreased with the concentrations of **11b** in PANC-1 cells ( $p < 0.01$ ), and the ratios of pPI3K/PI3K were decreased by 85% after the treatment of 4  $\mu\text{M}$  of **11b**. Similarly, **11b** also strongly inhibited the activity of Akt ( $p < 0.01$ ), and the pAkt/Akt relative expression was decreased by more than 50% at all five

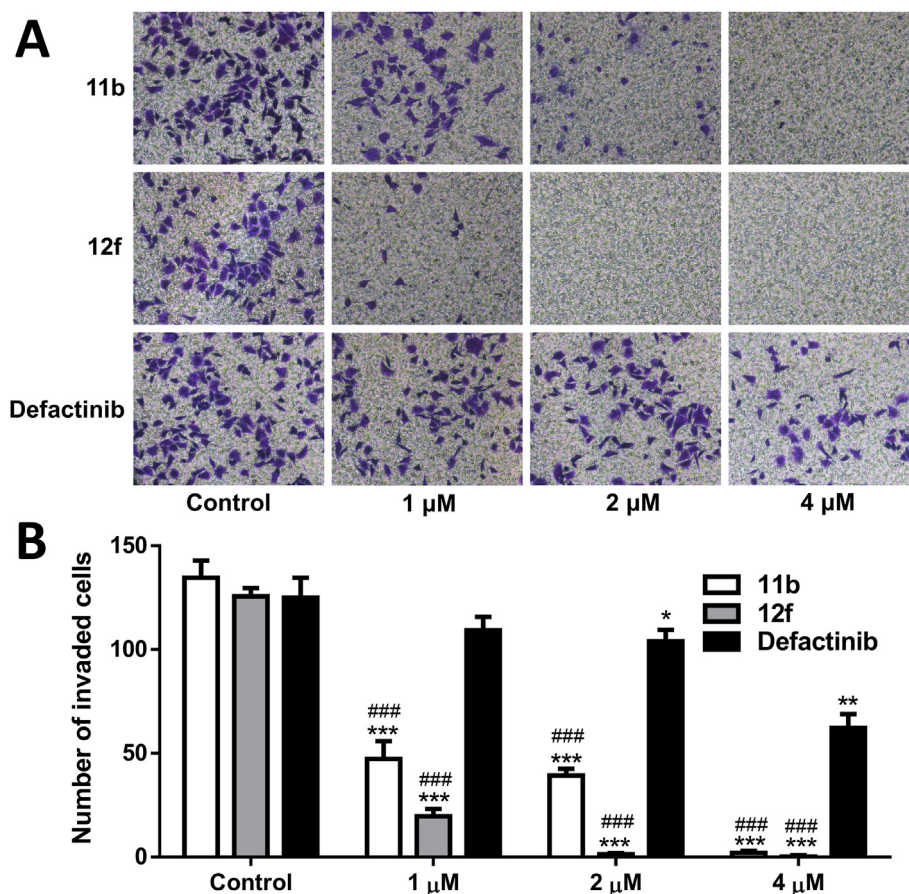


**Fig. 5.** The invasion suppressing effects of **11b** and **12f** against PANC-1 cells by transwell assay. (A) Suppressing effects of **11b** and **12f** (1, 2, 4  $\mu\text{M}$ ) on the invasion of PANC-1 cells ( $\times 100$ ). (B) Quantitative analysis of the invasion. \*:  $p < 0.05$ , \*\*:  $p < 0.01$ , \*\*\*:  $p < 0.001$ , vs. control; ###:  $p < 0.001$ , vs. defactinib at the same concentration;  $n = 3$ .

concentrations. Since the G2/M phase arrest and apoptosis were observed in PANC-1 cells after **11b** treatment, the expressions of cyclin D1 and apoptotic-related proteins (Bax and Bcl-2) were then investigated. Results showed that the levels of cyclin D1 were obviously decreased ( $p < 0.05$ ), whereas the ratios of Bax/Bcl-2 were significantly enhanced ( $p < 0.01$ ) at the concentrations higher than 0.25  $\mu\text{M}$ , which were consistent with the former studies.

For compound **12f**, a much stronger inhibitory activities were observed against these proteins in PANC-1 cells (Fig. 10B). **12f** treatment severely impaired the pFAK/FAK, pPI3K/PI3K, and pAkt/Akt relative expressions, suggesting the inhibitory of FAK/PI3K/Akt pathway. Meanwhile, the expression of cyclin D1 was significantly impaired ( $p < 0.01$ ), and the ratio of Bax/Bcl-2 was increased markedly ( $p < 0.05$ ).

#### 2.2.10. Kinase selectivity study

The kinase profiling of **12f** in a kinase profiling panel was then carried out against tyrosine kinase families, and a total of 74 tyrosine kinases were selected (Fig. 11). Results revealed that, apart from FAK, the activities of 7 tyrosine kinases were also significantly inhibited by **12f** at the concentration of 1  $\mu\text{M}$ , with the inhibition rate higher than 90%. Specifically, these kinases consist of another FAK family member (PYK2) [32], three tropomyosin receptor kinases (TRKA/B/C) [33], and three Janus kinases (JAK2/3 [34] and TYK2 [35]), all of which are involved in the regulation of cancer progression. To better understand the selectivity, the inhibitory effect of **11b** and **12f** against these tyrosine kinases were further

evaluated. As listed in Table 2, **12f** effectively inhibited these tyrosine kinases with  $\text{IC}_{50}$  values ranging from 17.89 to 39.44 nM. Compared with FAK ( $\text{IC}_{50} = 1.87$  nM), the  $\text{IC}_{50}$ s of **12f** increased approximately 13-, 10-, 21-, 16-, 10-, 11-, 12-fold for PYK2, TRKA, TRKB, TRKC, JAK2, JAK3, TYK2, respectively, indicating the good selectivity of **12f**. For compound **11b**, although the inhibitory activity against these kinases was obviously decreased, the selectivity was improved to higher than 11-fold for all 7 tyrosine kinases over FAK. By contrast, defactinib displayed a mild inhibitory effect but better selectivity (>22-fold) against 7 tyrosine kinases than **11b** and **12f**.

#### 2.3. Anti-angiogenesis activity

HUVEC (human umbilical vein endothelial cells) is a useful model for studying physiological and pathological processes of the vasculature *in vitro*, and is widely studied human endothelial cell type in angiogenesis [36–38]. All the synthesized compounds (**11a–11k** and **12a–12l**) were evaluated for the antiproliferative effect against HUVECs (Table 1). The result showed that most of the molecules displayed good activities, and compounds **11b** and **12f** also effectively inhibited the proliferation of HUVECs, with  $\text{IC}_{50}$  values of 2.29 and 0.18  $\mu\text{M}$ , respectively. Meanwhile, the vascular endothelial growth factor receptor 2 (VEGFR2) inhibitory effect was then investigated, and the results showed that **11b** and **12f** severely impaired the activity of VEGFR2, with  $\text{IC}_{50}$ s of 146.8 and 291.8  $\mu\text{M}$ , respectively. Further anti-angiogenesis analysis was then performed on these two compounds.

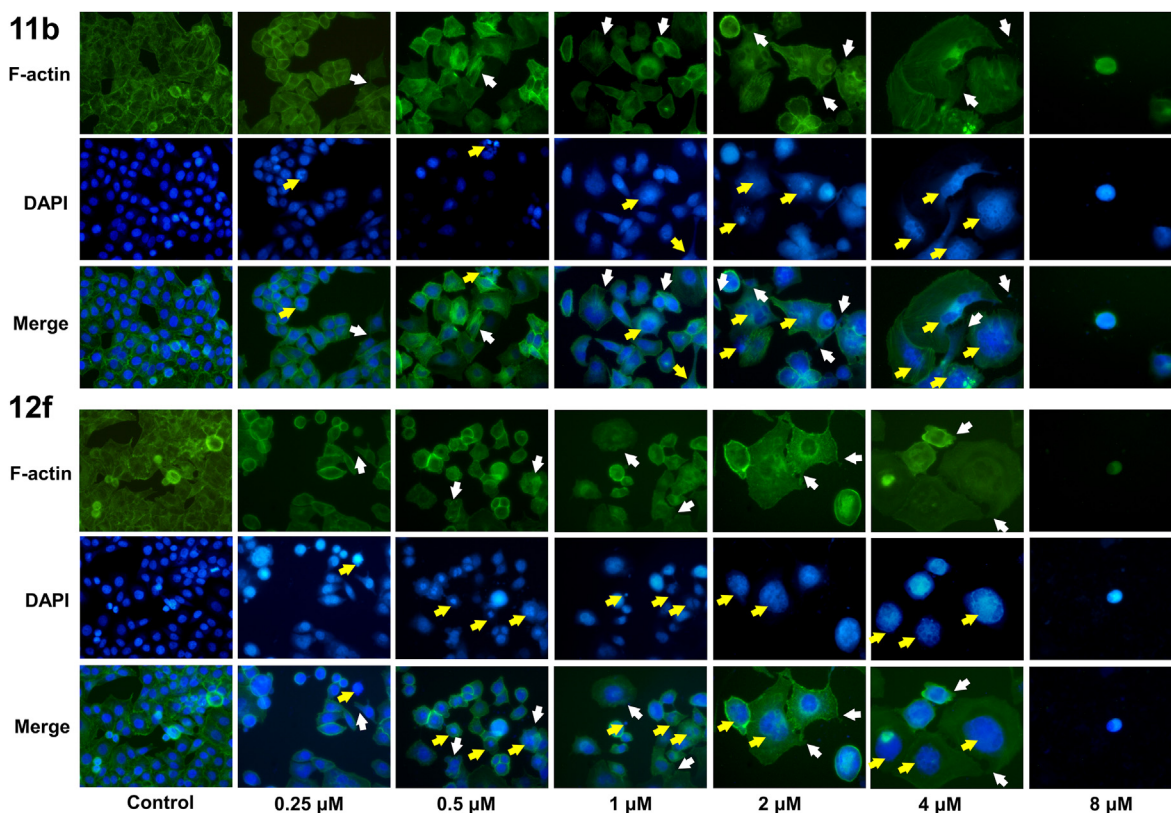


**Fig. 6.** Morphological analysis of morphological changes induced by **11b** and **12f** in PANC-1 cells. Immunofluorescence staining of  $\beta$ -catenin expression in PANC-1 cells. F-actin proteins were stained with FITC-phalloidin (green) and nuclei were stained with DAPI (blue) ( $\times 100$ ). Yellow arrows, nuclear damage; white arrows, cytoskeleton disruption.

### 2.3.1. Migration assay

Migration of vascular endothelial cell is an important process for angiogenesis, and inhibiting the migration of HUVECs will effectively suppress cancer metastasis. Therefore, the migration inhibitory effects of **11b** and **12f** on HUVECs were explored by cell-based scratch assay. Results revealed that the scratched area in the DMSO groups were almost covered after 24 h (Fig. 12A), and the migration rates were 88.21% (Fig. 12B). By contrast, the cells treated with **11b** and **12f** exhibited slower recovery of the scratched areas with the increase in concentrations (0.5, 1, 2, 4, and 8  $\mu$ M). The migration rates of **11b** and **12f** were much lower than defactinib at the concentrations higher than 1  $\mu$ M ( $p < 0.05$ ). In particular, only negligible cells covered the blank areas for **11b** and **12f** at 8  $\mu$ M, and the migration rates were 8.22% and 6.08%, respectively, indicating strong inhibitory effect against the migration of HUVECs.

### 2.3.2. Tube formation of HUVECs

Neovascularization plays a key role in cancer growth, and HUVEC tube formation assay is a commonly used method to evaluate the ability of endothelial cells to form capillary-like structure [39]. HUVEC tube formation assay was then used to investigate the inhibitory effect of **11b** and **12f** on angiogenesis. As shown in Fig. 13A, integrated tubes on the Matrigel matrix were formed in the control group, while the tubes were fragmentary after adding 1, 2, 4  $\mu$ M of **11b** or **12f**. The HUVEC tube length, tube area and number of branch points were obviously suppressed with increasing doses (Fig. 13A). Statistical analysis revealed that, compared to the control group, the HUVEC tube forming capacities were significantly inhibited by **11b** and **12f** at the concentrations of 2 and 4  $\mu$ M ( $p < 0.001$ , Fig. 13B), with almost no tube structure, which were more effective than defactinib ( $p < 0.001$ ).

### 2.3.3. Anti-angiogenesis in zebrafish embryos

Zebrafish embryo is a useful model to study human diseases, and transgenic zebrafish models expressing green fluorescent protein (GFP) in vascular endothelial cells are always used in studying angiogenesis *in vivo* [40]. **11b** and **12f** were incubated with the transgenic friend leukemia integration-1 (*fli-1*): enhanced GFP zebrafish embryos (Fig. 14). Results revealed that intersegmental vessels (ISV), dorsal aorta (DA), posterior cardinal vein (PCV), and dorsal longitudinal anastomotic vessels (DLAV) were clearly observed in newly born transgenic zebrafish embryos of the control group, indicating normal vessel developments. In contrast, for zebrafish embryos treated with **11b** and **12f**, DLAV and ISV formations were significantly reduced with concentrations increasing, and only scattered or fragmentary blood vessels were observed at 1 and 2  $\mu$ M, indicating strong anti-angiogenic effects of the two compounds *in vivo*.

## 3. Conclusion

In conclusion, a series of *N*-alkylbenzamide-substituted DAPYs were designed, synthesized, and evaluated for their anti-cancer and anti-angiogenesis activities. Most compounds effectively suppressed the enzymatic activities of FAK *in vitro*. Among these inhibitors, the most effective compounds **11b** and **12f** also exhibited strong antiproliferative activities against seven human cancer cell lines, including the two FAK-overexpressing pancreatic cancers PANC-1 and BxPC-3 cells. Moreover, **11b** and **12f** remarkably suppressed the colony formation, migration, and invasion of PANC-1 cells in a dose-dependent manner. Flow cytometry assay proved that **11b** and **12f** exerted anti-cancer effect by inducing the apoptosis of PANC-1 cells and arresting the cell cycle in G2/M

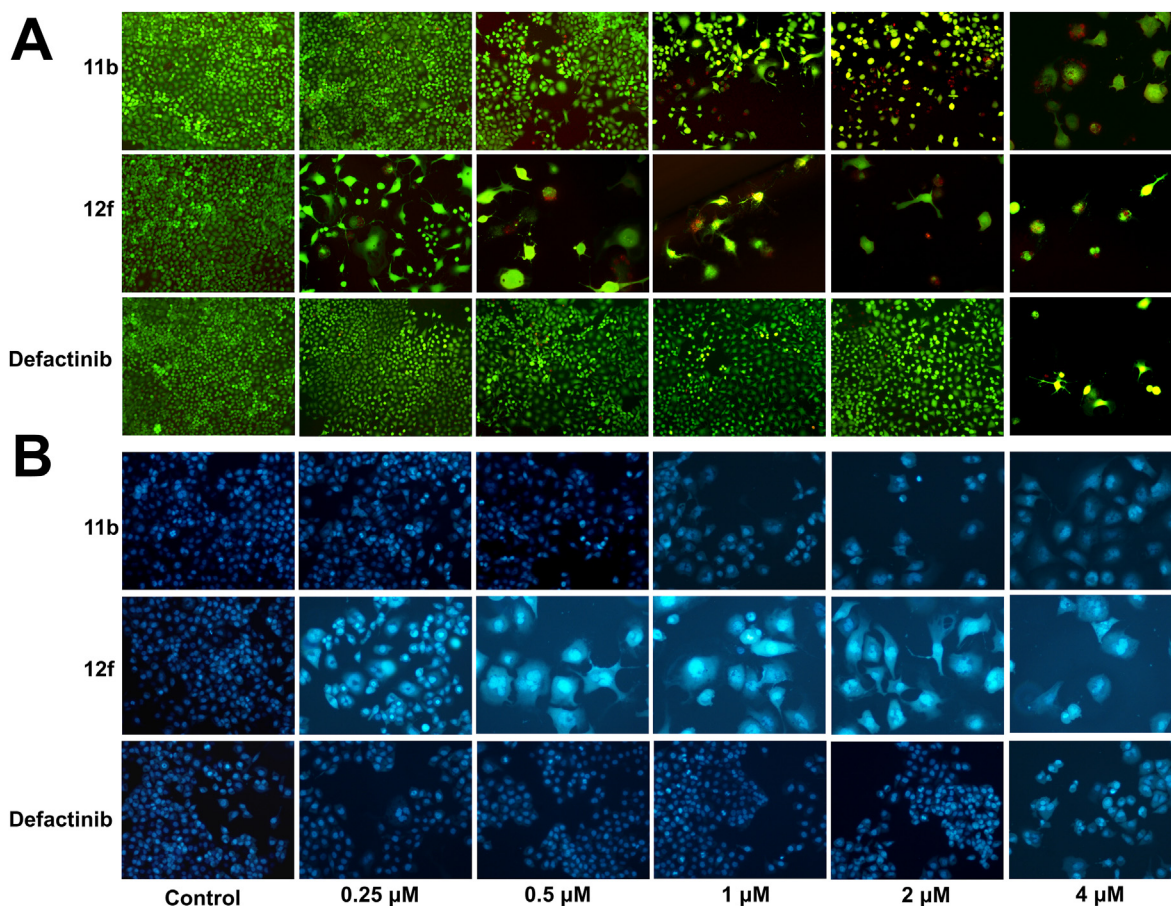


**Fig. 7.** Effects of compounds **11b** and **12f** on the apoptosis of PANC-1 cells. (A) Figures of PANC-1 cells stained with fluorescein diacetate (FDA)/propidium iodide (PI) ( $\times 100$ ). (B) Figures of PANC-1 cells stained with Hoechst 33258 ( $\times 100$ ).

phase. Both of two compounds effectively inhibited the FAK/PI3K/Akt signal pathway and significantly decreased the expression of cyclin D1 and Bcl-2. Further anti-angiogenesis studies showed that **11b** and **12f** effectively inhibited the antiproliferative, migration, and tube formation of HUVECs. *In vivo*, these two compounds also significantly inhibited the angiogenesis of zebrafish embryos. Therefore, **11b** and **12f** are considered promising candidates for further preclinical studies.

## 4. Experimental section

### 4.1. Chemistry

All analytical grade reagents and chemicals were purchased from commercial suppliers. The positive control defactinib were purchased from Bide Pharmatech Ltd. (China).  $^1\text{H}$  NMR and  $^{13}\text{C}$  NMR spectra were recorded on JEOL spectrometer (400 MHz) using  $\text{CDCl}_3$  or dimethyl sulfoxide ( $\text{DMSO}-d_6$ ) as solvents with the internal standard of TMS. High resolution mass spectrum (HRMS) was recorded on a Bruker UHPLC-MicroQ-TOF-II. All final compounds were purified to >95% purity as determined by HPLC (Dionex Ultimate 3000, USA) analysis using the following methods. Purity analysis of final compounds was performed through an ACE Excel-5- $\text{C}_{18}$  (particle size = 5  $\mu\text{m}$ , pore size = 4.6 nm, dimensions = 250 mm) column. The injection volume was 10  $\mu\text{L}$  with a gradient of 5–95% methanol/water. The flow rate was 1.0 mL/min and each analysis lasted for 15 min. The percentage of each solvent and retention times ( $R_{\text{T,HPLC}}$ ) and purity data (%) are

displayed in the analytical data of the respective compounds. All melting points were obtained on a WRS-2 Microcomputer Melting Point Apparatus.

### 4.2. General procedure for the synthesis of compounds **11a–11k** and **12a–12l**

#### 4.2.1. *N*-methyl-4-nitrobenzamide (**10b**)

4-Nitrobenzoic acid (0.50 g, 2.99 mmol) was dissolved in oxalyl chloride (25 mL) and refluxed for 3 h, then cooled to room temperature and concentrated under vacuum to afford a crude residue. To an ice-cooled solution of residue in DCM (100 mL) was added dropwise  $\text{Et}_3\text{N}$  (0.91 g, 8.97 mmol) and 40%  $\text{CH}_3\text{NH}_2$  (0.14 g, 2.6 mmol). The resulting mixture was stirred at room temperature for 1 h (monitored by TLC), and the mixture was evaporated to dryness in vacuum. The crude residue was applied to silica gel column chromatography (1:4 v/v ethyl acetate/petroleum ether) to afford a white solid (0.26 g, 57%). m. p. 216.0–220.1  $^\circ\text{C}$ ;  $^1\text{H}$  NMR (400 MHz,  $\text{DMSO}-d_6$ )  $\delta$  8.66 (s, 1H), 8.25 (d,  $J = 8.4$  Hz, 2H), 8.01 (d,  $J = 8.4$  Hz, 2H), 2.78 (d,  $J = 4.4$  Hz, 3H).  $^{13}\text{C}$  NMR (100 MHz,  $\text{DMSO}-d_6$ )  $\delta$  165.49, 149.49, 140.71, 129.01, 124.07, 26.87.  $R_{\text{T,HPLC}} = 12.297$  min, purity >99%.

#### 4.2.2. 4-Amino-*N*-methylbenzamide (**10c**)

To a solution of compound **10b** (1.00 g, 5.55 mmol) in ethyl acetate (50 mL) was added  $\text{SnCl}_2 \cdot 2\text{H}_2\text{O}$  (6.26 g, 27.75 mmol). The resulting mixture was heated under reflux for 3 h (monitored by TLC). Then the mixture was cooled to room temperature, brought to

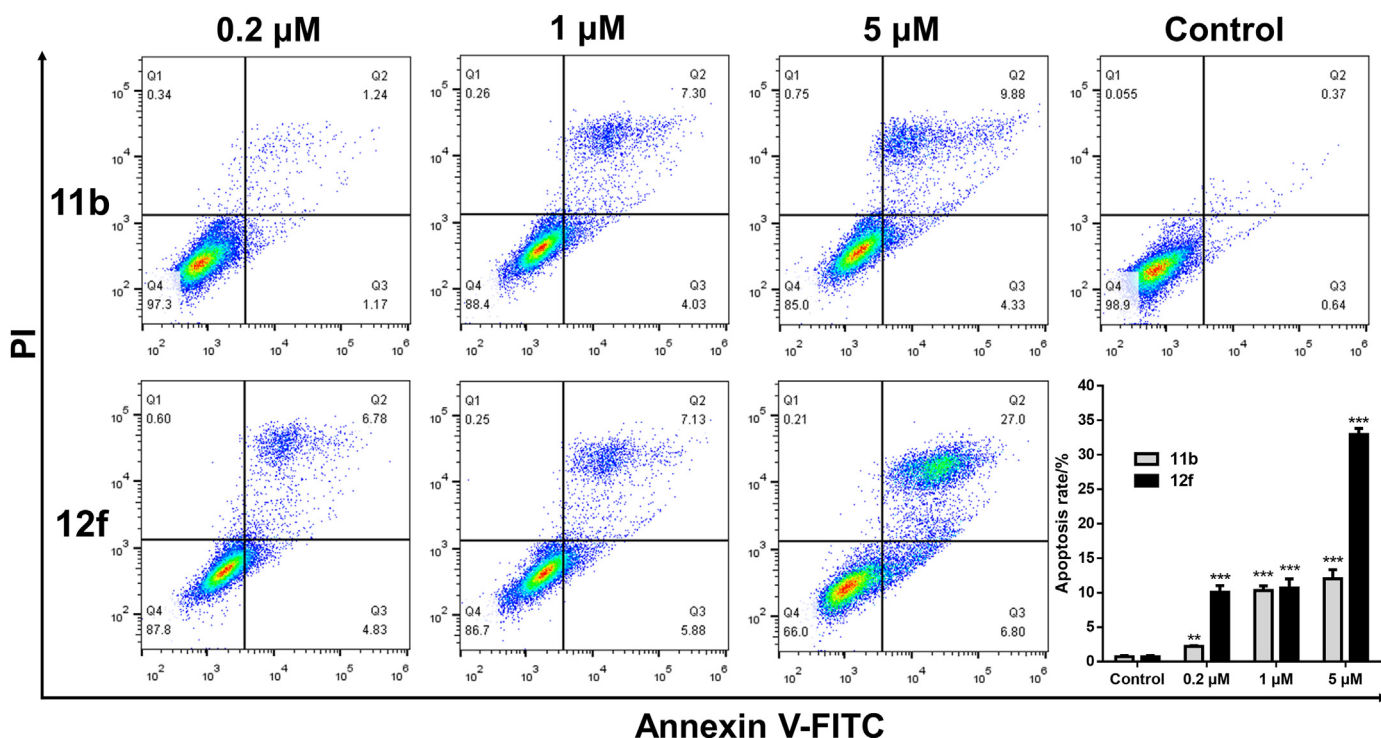


**Fig. 8.** Flow cytometry analysis of apoptosis induction in PANC-1 cells treated with compounds **11b** and **12f** (0.2, 1, 5 μM) for 48 h, and untreated cells (control) as a control. The cells were stained with Annexin V-FITC and PI, followed by flow cytometry analysis. Histogram analysis of the apoptosis is shown in bottom right panel. \*\*:  $p < 0.01$ , \*\*\*:  $p < 0.001$ , vs. control.

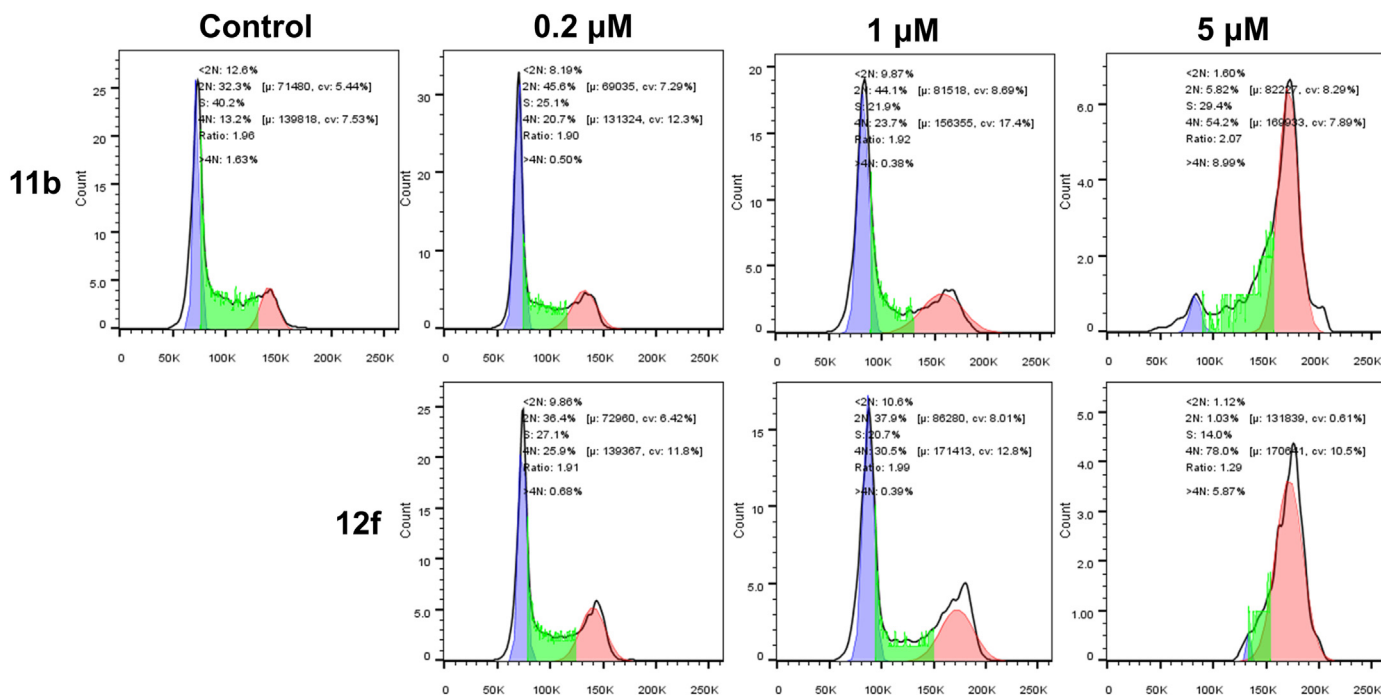


**Fig. 9.** Cell cycle analysis of PANC-1 cells treated with **11b** and **12f** (0.2, 1, 5 μM) for 24 h by flow cytometry assay.

pH9 by adding anhydrous sodium carbonate, and concentrated under reduced pressure to afford the crude product. The residue was applied to silica gel column chromatography (1:2 v/v ethyl acetate/petroleum ether) to afford a white solid (0.61 g, 75%). m. p. 181.5–181.8 °C;  $^1\text{H NMR}$  (400 MHz,  $\text{DMSO-}d_6$ )  $\delta$  7.85 (s, 1H), 7.52 (d,

$J = 8.4$  Hz, 2H), 6.50 (d,  $J = 8.4$  Hz, 2H), 5.46 (s, 1H), 2.69 (d,  $J = 4.4$  Hz, 3H).  $^{13}\text{C NMR}$  (100 MHz,  $\text{DMSO-}d_6$ )  $\delta$  167.32, 151.92, 129.06, 129.00, 122.07, 113.16, 113.14, 26.62.  $R_{\text{T,HPLC}} = 7.340$  min, purity >99%.

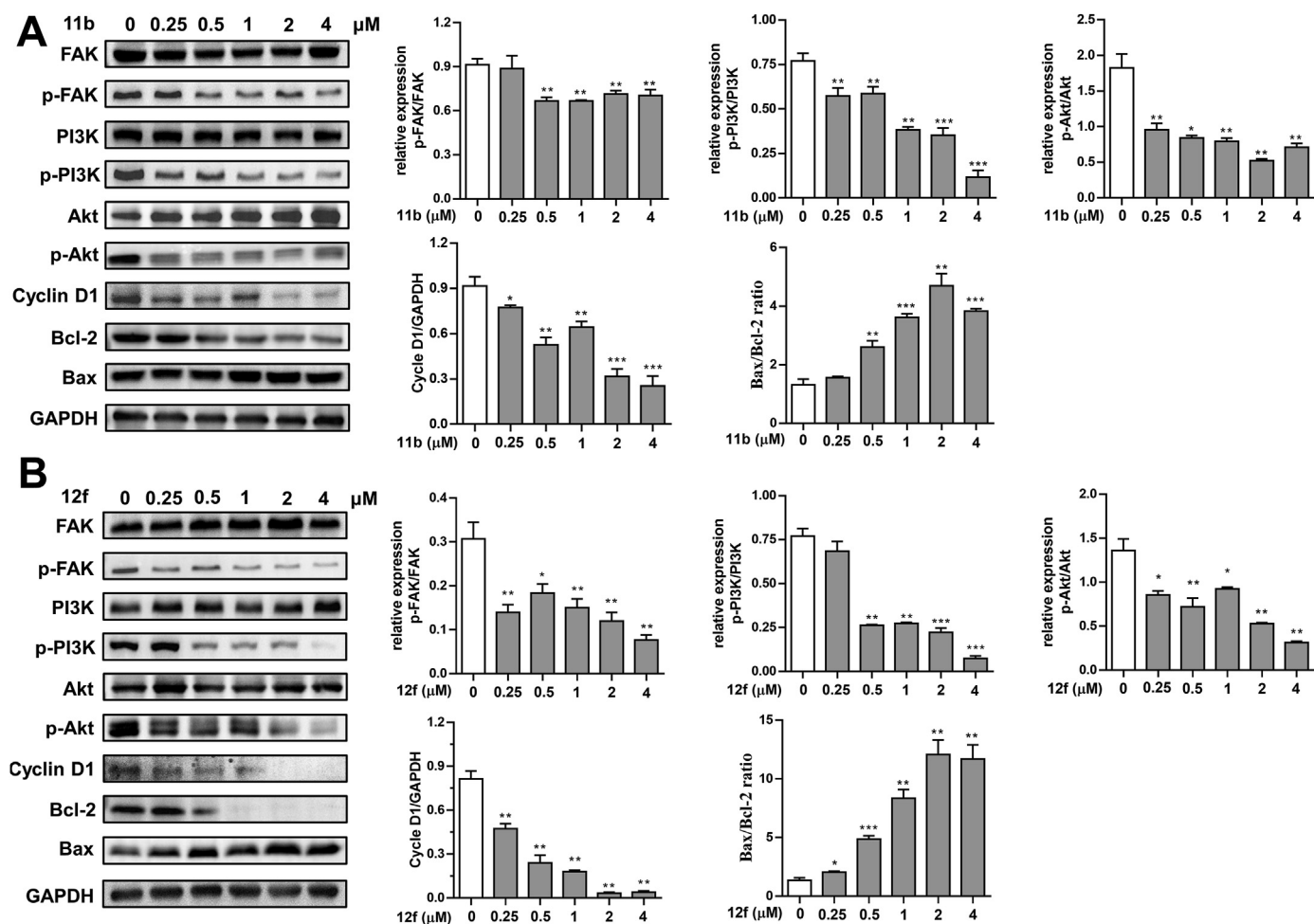


**Fig. 10.** Effect of **11b** (A) and **12f** (B) on the FAK/PI3K/AKT signaling pathway (FAK, pFAK, PI3K, pPI3K, Akt, and pAkt), cyclin D1, and apoptotic-related proteins (Bax and Bcl-2) in PANC-1 cells. \*:  $p < 0.05$ , \*\*:  $p < 0.01$ , \*\*\*:  $p < 0.001$ , vs. control.

#### 4.2.3. 4-((4-Chloro-5-(trifluoromethyl)pyrimidin-2-yl)amino)-N-methylbenzamide (**10d**)

To an ice-cooled solution of 2,4-dichloro-5-(trifluoromethyl)pyrimidine (0.83 g, 3.83 mmol) in DCM/*t*-BuOH (1:1) was added  $ZnBr_2$  (2.24 g, 9.95 mmol). The mixture was stirred at 0 °C for 30 min. To this mixture was added compound **9** (0.50 g, 3.33 mmol) and  $Et_3N$  (0.74 g, 7.27 mmol). The resulting mixture was stirred at room temperature for 21 h and then concentrated under reduced pressure. The oily residue was applied to silica gel column chromatography (1:2 v/v ethyl acetate/petroleum ether) to afford a white solid (0.65 g, 51%). m. p. 221.7–224.1 °C;  $^1H$  NMR (400 MHz, DMSO- $d_6$ )  $\delta$  10.81 (s, 1H), 8.84 (s, 1H), 8.26 (d,  $J = 4.4$  Hz, 1H), 7.83–7.76 (m, 4H), 2.78 (d,  $J = 4.4$  Hz, 3H).  $^{13}C$  NMR (100 MHz, DMSO- $d_6$ )  $\delta$  166.65, 160.96, 158.26, 141.41, 130.06, 128.30, 120.01, 112.66, 112.33, 26.43;  $R_{T,HPLC} = 13.34$  min, purity > 98%.

#### 4.2.4. 4-((4-((2-Fluorobenzyl)amino)-5-(trifluoromethyl)pyrimidin-2-yl)amino)-N-methylbenzamide (**11a**)

The synthesized intermediate **10** (100 mg, 0.3 mmol), 1-(bromomethyl)-2-fluorobenzene (113 mg, 0.6 mmol), and *N,N*-diisopropylethylamine (126 mg, 0.9 mmol) were dissolved in  $CH_3CN$  (15 mL), and the mixture was stirred at 90 °C for 12 h (monitored by TLC). After removal of  $CH_3CN$  using a rotary evaporator, the reaction mixture was applied to silica gel column chromatography (1:6 v/v ethyl acetate/petroleum ether) to afford a white solid (79 mg, 63%). m. p. 242.8–244.4 °C;  $^1H$  NMR (400 MHz, DMSO- $d_6$ )  $\delta$  9.77 (s, 1H),

8.28 (s, 1H), 8.16 (d,  $J = 4.4$  Hz, 1H), 7.74 (t,  $J = 7.2$  Hz, 1H), 7.63 (d,  $J = 8.8$  Hz, 2H), 7.58 (d,  $J = 7.6$  Hz, 2H), 7.31–7.20 (m, 3H), 7.14 (t,  $J = 7.2$  Hz, 1H), 4.76 (d,  $J = 6.4$  Hz, 2H), 2.76 (d,  $J = 4.4$  Hz, 3H).  $^{13}C$  NMR (100 MHz, DMSO- $d_6$ )  $\delta$  166.77, 161.66, 161.13, 159.24, 158.64, 142.92, 129.11, 129.02, 128.00, 126.76, 126.53, 126.39, 124.93, 124.89, 124.08, 118.54, 115.70, 115.49, 26.71. HRMS (ESI) calcd for  $C_{20}H_{17}F_4N_5O$   $[M+H]^+$ : 420.1442; found: 420.1440.  $R_{T,HPLC} = 6.44$  min, purity > 95%. The same procedure was also followed for the synthesis of **11b–11k**, **12a–12l**.

#### 4.2.5. 4-((4-((2-chlorobenzyl)amino)-5-(trifluoromethyl)pyrimidin-2-yl)amino)-N-methylbenzamide (**11b**)

White solid; 58% yield; m. p. 235.8–236.9 °C;  $^1H$  NMR (400 MHz, DMSO- $d_6$ )  $\delta$  9.88 (s, 1H), 8.32 (s, 1H), 8.23 (d,  $J = 4.4$  Hz, 1H), 7.89 (s, 1H), 7.61 (d,  $J = 8.8$  Hz, 2H), 7.55–7.49 (m, 3H), 7.34–7.26 (m, 2H), 7.19 (dd,  $J = 6.8, 2.4$  Hz, 1H), 4.75 (d,  $J = 5.6$  Hz, 2H), 2.76 (d,  $J = 4.4$  Hz, 3H).  $^{13}C$  NMR (100 MHz, DMSO- $d_6$ )  $\delta$  166.73, 161.14, 158.69, 158.68, 155.44, 155.39, 142.89, 136.51, 132.10, 129.69, 128.87, 128.04, 128.02, 127.76, 127.37, 126.81, 124.12, 118.40, 26.70. HRMS (ESI) calcd for  $C_{20}H_{17}ClF_3N_5O$   $[M+H]^+$ : 436.1146; found: 436.1147.  $R_{T,HPLC} = 6.37$  min, purity > 96%.

#### 4.2.6. 4-((4-((2-bromobenzyl)amino)-5-(trifluoromethyl)pyrimidin-2-yl)amino)-N-methylbenzamide (**11c**)

White solid; 47% yield; m. p. 258.8–261.4 °C;  $^1H$  NMR (400 MHz, DMSO- $d_6$ )  $\delta$  9.77 (s, 1H), 8.30 (s, 1H), 8.13 (d,  $J = 4.8$  Hz, 1H), 7.78 (t,

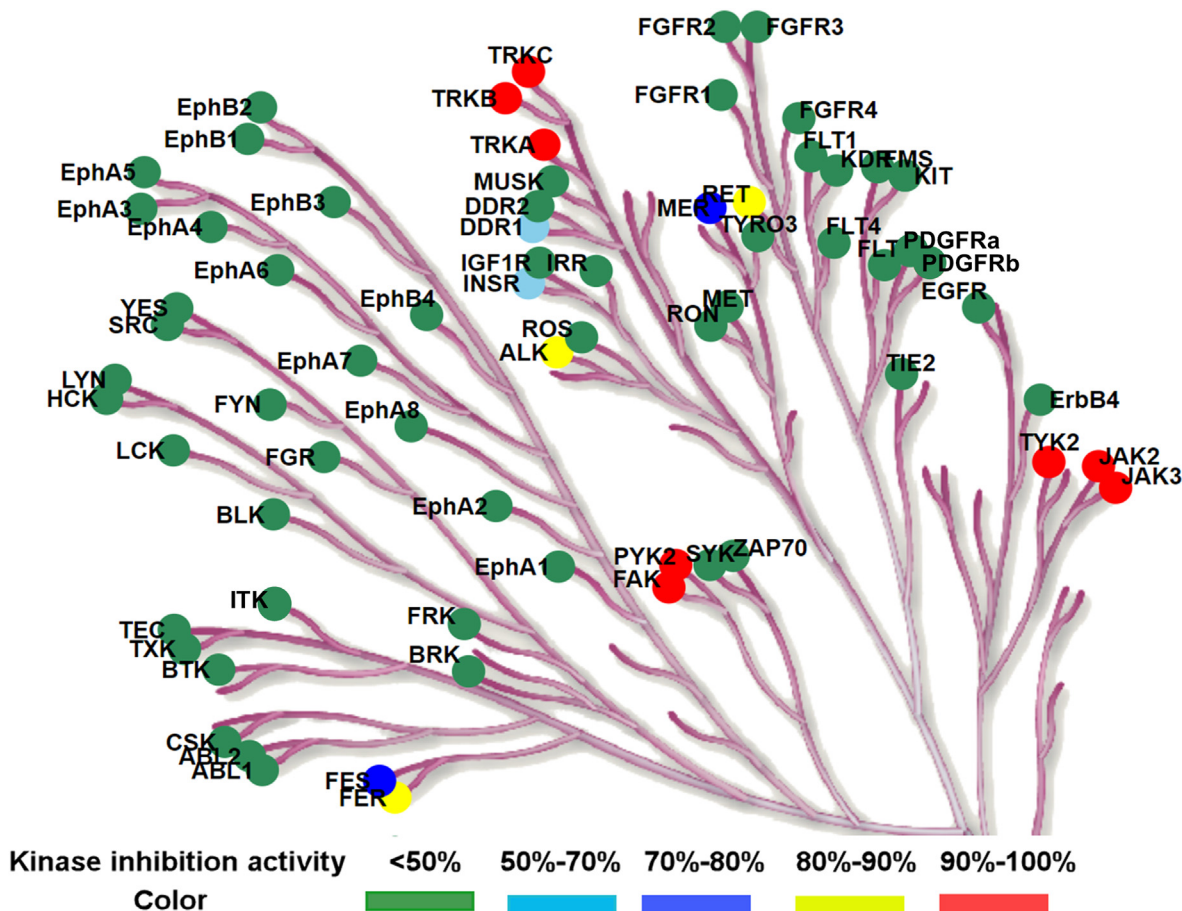


Fig. 11. Selectivity profiles of **12f** against the tyrosine kinase families at 1  $\mu\text{mol/L}$ . The kinome tree illustrations were generated by KinMap (<http://www.kinhub.org/kinmap/>).

**Table 2**  
Inhibitory activities of compounds **11b** and **12f** against seven tyrosine kinases.

Compound	Enzymatic activity ( $\text{IC}_{50}$ , nM)						
	PYK2	TRKA	TRKB	TRKC	JAK2	JAK3	TYK2
<b>11b</b>	116.2	31.54	102.72	102.12	36.97	44.18	39.07
<b>12f</b>	24.47	18.01	39.44	30.09	17.89	20.05	21.94
<b>Defactinib</b>	87.41	26.58	54.87	57.83	28.21	114.9	129.01

$J = 4.8$  Hz, 1H), 7.68 (d,  $J = 8$  Hz, 1H), 7.61 (d,  $J = 8.8$  Hz, 2H), 7.50 (d,  $J = 8.8$  Hz, 2H), 7.34 (t,  $J = 7.6$  Hz, 1H), 7.22–7.16 (m, 2H), 4.70 (d,  $J = 6.4$  Hz, 2H), 2.76 (s, 3H).  $^{13}\text{C}$  NMR (100 MHz,  $\text{DMSO}-d_6$ )  $\delta$  166.84, 161.18, 158.74, 155.43, 142.85, 137.95, 132.92, 129.14, 128.17, 128.06, 127.64, 126.81, 124.13, 122.40, 118.51, 45.04, 26.64. HRMS (ESI) calcd for  $\text{C}_{20}\text{H}_{17}\text{BrF}_3\text{N}_5\text{O}$   $[\text{M}+\text{H}]^+$ : 480.0647, 482.0626; found: 480.0536, 482.0527.  $R_{\text{T,HPLC}} = 6.37$  min, purity >91%.

#### 4.2.7. 4-((4-((3-fluorobenzyl)amino)-5-(trifluoromethyl)pyrimidin-2-yl)amino)-*N*-methylbenzamide (**11d**)

White solid; 40% yield; m. p. 232.3–236.4  $^{\circ}\text{C}$ ;  $^1\text{H}$  NMR (400 MHz,  $\text{DMSO}-d_6$ )  $\delta$  9.87 (s, 1H), 8.27 (d,  $J = 9.2$  Hz, 2H), 7.93 (s, 1H), 7.68–7.59 (m, 4H), 7.39 (dd,  $J = 14.4, 7.2$  Hz, 1H), 7.18 (d,  $J = 7.2$  Hz, 1H), 7.12–7.03 (m, 2H), 4.68 (s, 2H), 2.76 (d,  $J = 3.7$  Hz, 3H).  $^{13}\text{C}$  NMR (100 MHz,  $\text{DMSO}-d_6$ )  $\delta$  166.79, 163.98, 161.56, 161.15, 158.50, 143.12, 143.05, 142.89, 130.86, 130.78, 128.06, 128.04, 126.74, 123.08, 118.77, 114.09, 113.88, 43.77, 26.71. HRMS (ESI) calcd for  $\text{C}_{20}\text{H}_{17}\text{F}_4\text{N}_5\text{O}$   $[\text{M}+\text{H}]^+$ : 420.1442; found: 420.1444.  $R_{\text{T,HPLC}} = 6.53$  min, purity >97%.

#### 4.2.8. 4-((4-((3-chlorobenzyl)amino)-5-(trifluoromethyl)pyrimidin-2-yl)amino)-*N*-methylbenzamide (**11e**)

White solid; 34% yield; m. p. 187.9–192.2  $^{\circ}\text{C}$ ;  $^1\text{H}$  NMR (400 MHz,  $\text{DMSO}-d_6$ )  $\delta$  9.89 (s, 1H), 8.29–8.26 (m, 2H), 7.94 (s, 1H), 7.72–7.61 (m, 4H), 7.40–7.28 (m, 4H), 4.68 (d,  $J = 5.2$  Hz, 2H), 2.77 (d,  $J = 4.4$  Hz, 3H).  $^{13}\text{C}$  NMR (100 MHz,  $\text{DMSO}-d_6$ )  $\delta$  166.76, 161.17, 158.46, 155.39, 155.34, 142.86, 142.64, 133.53, 130.75, 128.12, 128.08, 127.20, 126.92, 126.75, 125.84, 124.07, 118.82, 43.73, 26.70. HRMS (ESI) calcd for  $\text{C}_{20}\text{H}_{17}\text{ClF}_3\text{N}_5\text{O}$   $[\text{M}+\text{H}]^+$ : 436.1146; found: 436.1144.  $R_{\text{T,HPLC}} = 6.56$  min, purity >97%.

#### 4.2.9. 4-((4-((3-bromobenzyl)amino)-5-(trifluoromethyl)pyrimidin-2-yl)amino)-*N*-methylbenzamide (**11f**)

White solid; 44% yield; m. p. 175.5–179.2  $^{\circ}\text{C}$ ;  $^1\text{H}$  NMR (400 MHz,  $\text{DMSO}-d_6$ )  $\delta$  9.88 (s, 1H), 8.29–8.25 (m, 2H), 7.93 (t,  $J = 4.8$  Hz, 1H), 7.70 (d,  $J = 8.8$  Hz, 2H), 7.62 (d,  $J = 8.4$  Hz, 2H), 7.50 (s, 1H), 7.42 (dt,  $J = 7.6, 1.6$  Hz, 1H), 7.36–7.29 (m, 2H), 4.67 (d,  $J = 5.6$  Hz, 2H), 2.76 (d,  $J = 4.4$  Hz, 3H).  $^{13}\text{C}$  NMR (100 MHz,  $\text{DMSO}-d_6$ )  $\delta$  166.93, 162.06, 158.69, 157.17, 154.07, 140.12, 130.51, 127.91, 127.43, 126.56, 126.18, 122.60, 120.65, 120.40, 110.97, 100.00, 55.76, 26.80. HRMS (ESI) calcd for  $\text{C}_{20}\text{H}_{17}\text{BrF}_3\text{N}_5\text{O}$   $[\text{M}+\text{H}]^+$ : 480.0647, 482.0626; found: 480.0616, 482.0598.  $R_{\text{T,HPLC}} = 6.54$  min, purity >97%.

#### 4.2.10. 4-((4-((4-fluorobenzyl)amino)-5-(trifluoromethyl)pyrimidin-2-yl)amino)-*N*-methylbenzamide (**11g**)

White solid; 45% yield; m. p. 211.4–214.5  $^{\circ}\text{C}$ ;  $^1\text{H}$  NMR (400 MHz,  $\text{DMSO}-d_6$ )  $\delta$  9.84 (s, 1H), 8.25–8.24 (m, 2H), 7.89 (t,  $J = 6$  Hz, 1H), 7.67 (d,  $J = 8.8$  Hz, 2H), 7.61 (d,  $J = 8.8$  Hz, 2H), 7.37–7.33 (m, 2H), 7.15 (t,

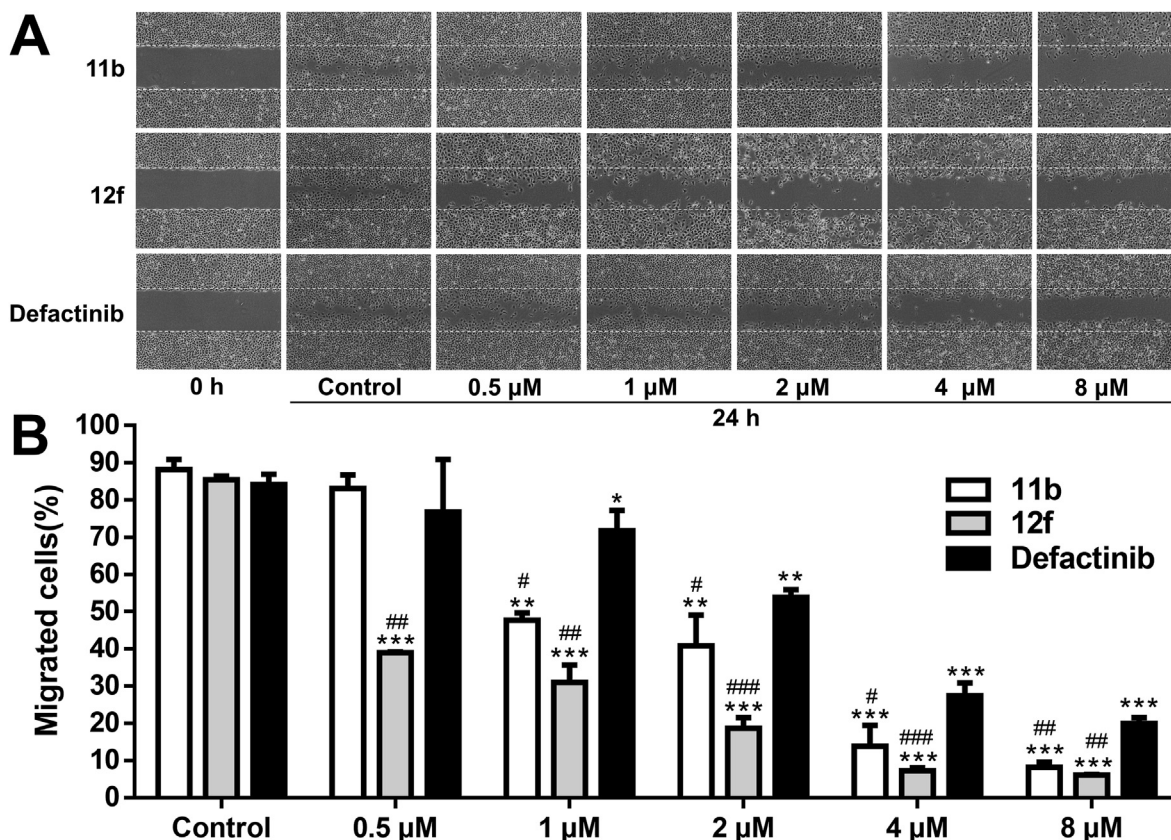


**Fig. 12.** Effects of compounds **11b** and **12f** on the migration of HUVEC cells *in vitro* determined by scratch assay. (A) Images of HUVEC cells migration inhibited by **11b** and **12f** ( $\times 40$ ). (B) Filled areas calculated by ImageJ software. \*:  $p < 0.05$ , \*\*:  $p < 0.01$ , \*\*\*:  $p < 0.001$ , vs. control group; #:  $p < 0.05$ , ##:  $p < 0.01$ , ###:  $p < 0.001$ , vs. defactinib at the same concentration;  $n = 3$ .

$J = 8.8$  Hz, 2H), 4.65 (d,  $J = 5.6$  Hz, 2H), 2.76 (d,  $J = 4.4$  Hz, 3H).  $^{13}\text{C}$  NMR (100 MHz,  $\text{DMSO-}d_6$ )  $\delta$  166.77, 162.79, 161.18, 160.38, 158.48, 155.29, 142.96, 136.07, 136.04, 129.03, 128.94, 128.08, 128.00, 126.76, 124.08, 118.77, 115.67, 115.46, 43.51, 26.70. HRMS (ESI) calcd for  $\text{C}_{20}\text{H}_{17}\text{F}_4\text{N}_5\text{O}$   $[\text{M}+\text{H}]^+$ : 420.1442; found: 420.1438.  $R_{\text{T,HPLC}} = 6.54$  min, purity >96%.

#### 4.2.11. 4-((4-((4-chlorobenzyl)amino)-5-(trifluoromethyl)pyrimidin-2-yl)amino)-*N*-methylbenzamide (**11h**)

White solid; 48% yield; m. p. 222.8–225.6 °C;  $^1\text{H}$  NMR (400 MHz,  $\text{DMSO-}d_6$ )  $\delta$  9.86 (s, 1H), 8.28 (m, 2H), 7.93 (t,  $J = 6$  Hz, 1H), 7.68 (d,  $J = 8.8$  Hz, 2H), 7.61 (d,  $J = 8.8$  Hz, 2H), 7.42–7.39 (m, 2H), 7.36–7.34 (m, 2H), 4.67 (d,  $J = 5.8$  Hz, 2H), 2.77–2.77 (m, 3H).  $^{13}\text{C}$  NMR (100 MHz,  $\text{DMSO-}d_6$ )  $\delta$  166.73, 161.17, 158.47, 155.33, 155.28, 142.92, 139.02, 131.69, 128.93, 128.78, 128.07, 128.02, 126.75, 124.07, 118.77, 43.63, 26.71. HRMS (ESI) calcd for  $\text{C}_{20}\text{H}_{17}\text{ClF}_3\text{N}_5\text{O}$   $[\text{M}+\text{H}]^+$ : 436.1146; found: 436.1136.  $R_{\text{T,HPLC}} = 6.47$  min, purity >97%.

#### 4.2.12. 4-((4-((4-bromobenzyl)amino)-5-(trifluoromethyl)pyrimidin-2-yl)amino)-*N*-methylbenzamide (**11i**)

White solid; 40% yield; m. p. 235.1–237.3 °C;  $^1\text{H}$  NMR (400 MHz,  $\text{DMSO-}d_6$ )  $\delta$  9.86 (s, 1H), 8.26 (d,  $J = 5.6$  Hz, 2H), 7.92 (t,  $J = 5.6$  Hz, 1H), 7.68 (d,  $J = 8.4$  Hz, 2H), 7.60 (d,  $J = 8.4$  Hz, 2H), 7.54 (d,  $J = 8.2$  Hz, 2H), 7.29 (d,  $J = 8.2$  Hz, 2H), 4.65 (d,  $J = 5.6$  Hz, 2H), 2.76 (d,  $J = 4.4$  Hz, 3H).  $^{13}\text{C}$  NMR (100 MHz,  $\text{DMSO-}d_6$ )  $\delta$  166.71, 161.17, 158.48, 155.34, 155.29, 142.91, 139.46, 131.69, 129.32, 128.07, 128.04, 126.76, 124.08, 120.16, 118.78, 43.69, 26.71. HRMS (ESI) calcd for  $\text{C}_{20}\text{H}_{17}\text{BrF}_3\text{N}_5\text{O}$   $[\text{M}+\text{H}]^+$ : 480.0647, 482.0626; found: 480.0576,

482.0560.  $R_{\text{T,HPLC}} = 13.88$  min, purity >99%.

#### 4.2.13. 4-((4-((2-methoxybenzyl)amino)-5-(trifluoromethyl)pyrimidin-2-yl)amino)-*N*-methylbenzamide (**11j**)

White solid; 46% yield; m. p. 259.6–260.8 °C;  $^1\text{H}$  NMR (400 MHz,  $\text{DMSO-}d_6$ )  $\delta$  9.81 (s, 1H), 8.28 (s, 1H), 8.22 (q,  $J = 4.4$  Hz, 1H), 7.65–7.51 (m, 5H), 7.23 (t,  $J = 7.2$  Hz, 1H), 7.06–7.04 (m, 2H), 6.89 (td,  $J = 7.2, 0.8$  Hz, 1H), 4.65 (d,  $J = 5.8$  Hz, 2H), 3.89 (s, 3H), 2.75 (d,  $J = 4.4$  Hz, 3H).  $^{13}\text{C}$  NMR (100 MHz,  $\text{DMSO-}d_6$ )  $\delta$  166.76, 161.17, 158.70, 157.03, 155.29, 155.24, 142.97, 128.23, 127.94, 127.92, 126.86, 126.31, 124.18, 120.65, 118.66, 110.76, 55.80, 26.70. HRMS (ESI) calcd for  $\text{C}_{21}\text{H}_{20}\text{F}_3\text{N}_5\text{O}$   $[\text{M}+\text{H}]^+$ : 432.1641; found: 432.1641.  $R_{\text{T,HPLC}} = 6.49$  min, purity >95%.

#### 4.2.14. 4-((4-((4-methoxybenzyl)amino)-5-(trifluoromethyl)pyrimidin-2-yl)amino)-*N*-methylbenzamide (**11k**)

White solid; 61% yield; m. p. 229.6–230.2 °C;  $^1\text{H}$  NMR (400 MHz,  $\text{DMSO-}d_6$ )  $\delta$  9.84 (s, 1H), 8.28–8.26 (m, 2H), 7.84 (s, 1H), 7.72–7.677 (m, 4H), 7.27 (d,  $J = 7.2$  Hz, 2H), 6.90 (dd,  $J = 8.8, 2$  Hz, 2H), 4.58 (d,  $J = 5.3$  Hz, 2H), 3.70 (d,  $J = 2.1$  Hz, 3H), 2.77 (d,  $J = 4.4$  Hz, 3H).  $^{13}\text{C}$  NMR (100 MHz,  $\text{DMSO-}d_6$ )  $\delta$  166.75, 161.18, 158.59, 158.44, 155.22, 155.16, 143.02, 131.79, 128.10, 127.93, 126.78, 124.10, 118.76, 114.21, 55.50, 43.56, 26.71. HRMS (ESI) calcd for  $\text{C}_{21}\text{H}_{20}\text{F}_3\text{N}_5\text{O}_2$   $[\text{M}+\text{H}]^+$ : 432.1641; found: 432.1623.  $R_{\text{T,HPLC}} = 6.45$  min, purity >98%.

#### 4.2.15. 4-((4-((4-fluorophenyl)amino)-5-(trifluoromethyl)pyrimidin-2-yl)amino)-*N*-methylbenzamide (**12a**)

White solid; 47% yield; m. p. 253.2–254.3 °C;  $^1\text{H}$  NMR

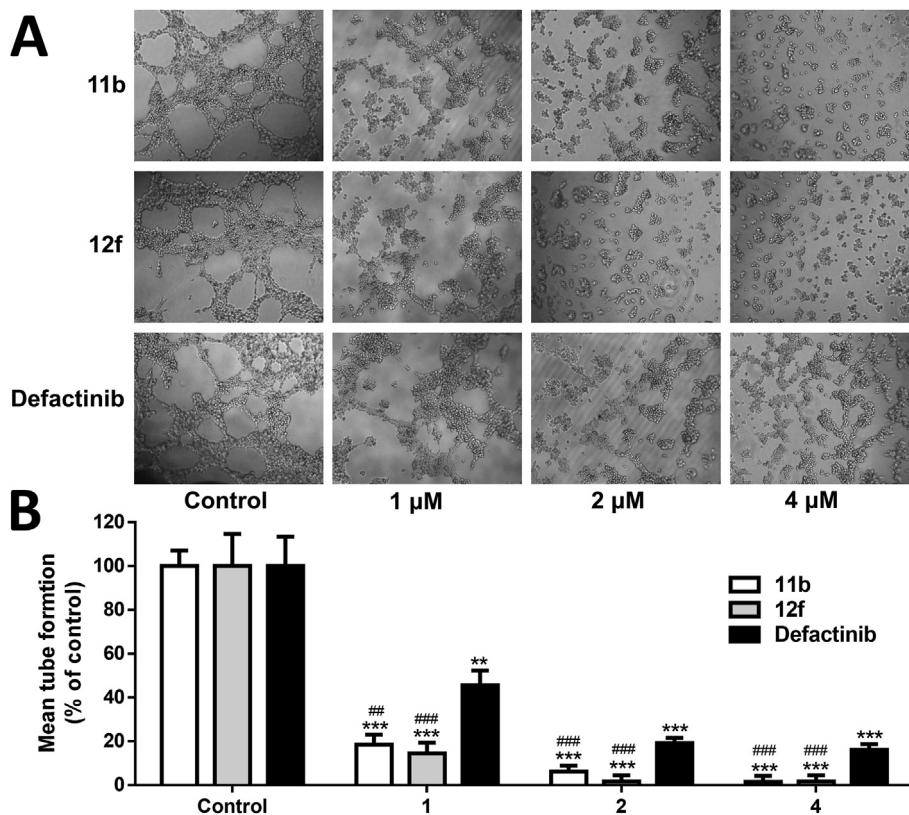


**Fig. 13.** Effects of compounds **11b** and **12f** on the tube formation of HUVECs *in vitro* ( $\times 100$ ). (A) Images for the tube-forming inhibitory activities for **11b** and **12f** (1, 2, 4, 8  $\mu\text{M}$ ) in HUVECs ( $\times 40$ ). (B) Statistical analysis for the tube-forming capability. \*\*:  $p < 0.01$ , vs. control; \*\*\*:  $p < 0.001$ , vs. control;  $n = 3$ .

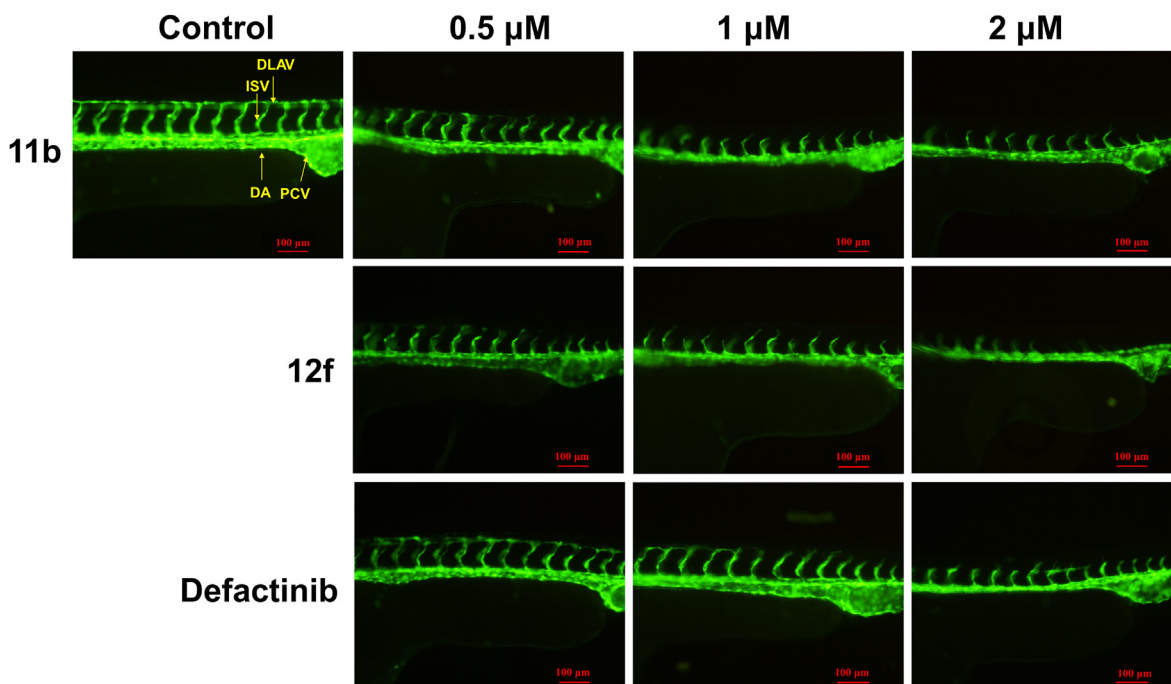


**Fig. 14.** Anti-angiogenic effect of compounds **11b** and **12f** in zebrafish embryos assay. Zebrafish embryos were incubated with **11b** or **12f** at 0.5, 1, and 2  $\mu\text{M}$  for 24 h.

(400 MHz,  $\text{DMSO-}d_6$ )  $\delta$  9.95 (s, 1H), 8.90 (s, 1H), 8.41 (s, 1H), 8.26 (d,  $J = 4.4$  Hz, 1H), 7.58 (s, 4H), 7.50–7.46 (m, 2H), 7.27 (t,  $J = 8.8$  Hz, 2H), 2.76 (d,  $J = 4.4$  Hz, 3H).  $^{13}\text{C}$  NMR (100 MHz,  $\text{DMSO-}d_6$ )  $\delta$  166.74, 160.88, 158.18, 156.20, 156.15, 142.79, 134.86, 128.83, 128.05, 127.95,

126.48, 123.80, 118.65, 115.77, 115.55, 26.68. HRMS (ESI) calcd for  $\text{C}_{19}\text{H}_{15}\text{F}_4\text{N}_5\text{O}$   $[\text{M}+\text{H}]^+$ : 406.1291; found: 406.1285.  $R_{\text{T,HPLC}} = 6.54$  min, purity >95%.

4.2.16. 4-((4-((2-chlorophenyl)amino)-5-(trifluoromethyl)pyrimidin-2-yl)amino)-N-methylbenzamide (**12b**)

White solid; 28% yield; m. p. 264.2–265.9 °C; <sup>1</sup>H NMR (400 MHz, DMSO-*d*<sub>6</sub>) δ 9.86 (s, 1H), 8.87 (s, 1H), 8.40 (s, 1H), 8.14 (d, *J* = 4.4 Hz, 1H), 7.64 (dd, *J* = 6.8, 2.0 Hz, 1H), 7.54 (d, *J* = 6.8 Hz, 1H), 7.49–7.45 (m, 4H), 7.39 (d, *J* = 8.4 Hz, 2H), 2.76 (d, *J* = 4.4 Hz, 3H). <sup>13</sup>C NMR (100 MHz, DMSO-*d*<sub>6</sub>) δ 166.76, 160.81, 158.53, 156.08, 142.82, 136.42, 131.03, 131.01, 130.22, 128.92, 128.36, 127.84, 126.55, 123.87, 118.26, 26.68. HRMS (ESI) calcd for C<sub>19</sub>H<sub>15</sub>F<sub>3</sub>N<sub>6</sub>O<sub>3</sub> [M+H]<sup>+</sup>: 422.0989; found: 422.0974. R<sub>T,HPLC</sub> = 6.55 min, purity >95%.

4.2.17. N-methyl-4-((4-((2-nitrophenyl)amino)-5-(trifluoromethyl)pyrimidin-2-yl)amino)benzamide (**12c**)

White solid; 43% yield; m. p. 251.0–253.1 °C; <sup>1</sup>H NMR (400 MHz, DMSO-*d*<sub>6</sub>) δ 10.08 (s, 1H), 9.56 (s, 1H), 8.52 (s, 1H), 8.26 (d, *J* = 4.4 Hz, 1H), 8.17 (d, *J* = 8.0 Hz, 1H), 8.02 (s, 1H), 7.85 (d, *J* = 8.0 Hz, 1H), 7.61–7.53 (m, 5H), 2.76 (d, *J* = 4.4 Hz, 3H). <sup>13</sup>C NMR (100 MHz, DMSO-*d*<sub>6</sub>) δ 166.67, 160.79, 157.74, 157.44, 156.69, 142.43, 134.90, 134.89, 133.36, 133.33, 128.45, 127.94, 125.82, 118.92, 118.76, 26.69. HRMS (ESI) calcd for C<sub>19</sub>H<sub>15</sub>F<sub>3</sub>N<sub>6</sub>O<sub>3</sub> [M+H]<sup>+</sup>: 433.1230; found: 433.1202. R<sub>T,HPLC</sub> = 6.38 min, purity >96%.

4.2.18. 4-((4-((4-aminophenyl)amino)-5-(trifluoromethyl)pyrimidin-2-yl)amino)-N-methylbenzamide (**12d**)

White solid; 18% yield; m. p. 266.5–268.9 °C; <sup>1</sup>H NMR (400 MHz, DMSO-*d*<sub>6</sub>) δ 9.71 (s, 1H), 8.45 (s, 1H), 8.29 (s, 1H), 8.09 (d, *J* = 4.8 Hz, 1H), 7.63–7.56 (m, 5H), 7.04 (d, *J* = 8.4 Hz, 2H), 6.63 (d, *J* = 8.4 Hz, 2H), 5.07 (s, 2H), 2.75 (d, *J* = 4.4 Hz, 3H). <sup>13</sup>C NMR (100 MHz, DMSO-*d*<sub>6</sub>) δ 166.96, 160.99, 158.59, 155.69, 147.29, 143.02, 128.01, 127.93, 126.94, 126.69, 124.00, 118.60, 114.23, 26.71. HRMS (ESI) calcd for C<sub>19</sub>H<sub>17</sub>F<sub>3</sub>N<sub>6</sub>O [M+H]<sup>+</sup>: 403.1488; found: 403.1478. R<sub>T,HPLC</sub> = 6.50 min, purity >96%.

4.2.19. 4-((4-((3-aminophenyl)amino)-5-(trifluoromethyl)pyrimidin-2-yl)amino)-N-methylbenzamide (**12e**)

White solid; 33% yield; m. p. 256.2–258.7 °C; <sup>1</sup>H NMR (400 MHz, CD<sub>3</sub>OD) δ 8.25 (s, 1H), 7.67–7.58 (m, 4H), 7.19–7.13 (m, 1H), 6.84 (s, 1H), 6.74 (dd, *J* = 8.0, 2.0 Hz, 1H), 6.67 (dd, *J* = 8.0, 2.0 Hz, 1H), 2.87 (s, 3H). <sup>13</sup>C NMR (100 MHz, CD<sub>3</sub>OD) δ 169.13, 160.56, 158.20, 154.94, 154.88, 147.90, 142.97, 138.72, 129.06, 127.53, 127.13, 126.13, 123.45, 118.37, 112.99, 100.00, 25.52. HRMS (ESI) calcd for C<sub>19</sub>H<sub>17</sub>F<sub>3</sub>N<sub>6</sub>O [M+H]<sup>+</sup>: 403.1488; found: 403.1478. R<sub>T,HPLC</sub> = 6.37 min, purity >98%.

4.2.20. 4-((4-((2-methoxyphenyl)amino)-5-(trifluoromethyl)pyrimidin-2-yl)amino)-N-methylbenzamide (**12f**)

White solid; 65% yield; m. p. 262.4–265.2 °C; <sup>1</sup>H NMR (400 MHz, DMSO-*d*<sub>6</sub>) δ 9.94 (s, 1H), 8.40 (s, 1H), 8.35 (s, 1H), 8.24 (d, *J* = 4.4 Hz, 1H), 7.83 (d, *J* = 8.8 Hz, 1H), 7.68 (d, *J* = 8.8 Hz, 1H), 7.59–7.55 (m, 4H), 7.32 (t, *J* = 8.0 Hz, 1H), 7.18 (d, *J* = 8.0 Hz, 1H), 7.03 (td, *J* = 7.6, 1.2 Hz, 1H), 3.78 (s, 3H), 2.76 (d, *J* = 4.4 Hz, 3H). <sup>13</sup>C NMR (100 MHz, DMSO-*d*<sub>6</sub>) δ 167.35, 167.17, 160.92, 158.27, 157.94, 142.78, 140.57, 130.08, 128.46, 128.37, 127.99, 127.28, 126.58, 123.89, 120.88, 119.06, 118.97, 100.00, 56.33, 26.76. HRMS (ESI) calcd for C<sub>20</sub>H<sub>18</sub>F<sub>3</sub>N<sub>6</sub>O<sub>2</sub> [M+H]<sup>+</sup>: 418.1485; found: 418.1484. R<sub>T,HPLC</sub> = 6.55 min, purity >95%.

4.2.21. 4-((4-((3-methoxyphenyl)amino)-5-(trifluoromethyl)pyrimidin-2-yl)amino)-N-methylbenzamide (**12g**)

White solid; 53% yield; m. p. 284.2–289.1 °C; <sup>1</sup>H NMR (400 MHz, DMSO-*d*<sub>6</sub>) δ 9.87 (s, 1H), 8.69 (s, 1H), 8.40 (s, 1H), 8.15 (d, *J* = 4.4 Hz, 1H), 7.61 (q, *J* = 8.8 Hz, 4H), 7.33 (t, *J* = 8.0 Hz, 1H), 7.09 (d, *J* = 8.0 Hz, 1H), 7.07 (t, *J* = 2.0 Hz, 1H), 6.85 (dd, *J* = 8.4, 2.4 Hz, 1H), 3.75 (s, 3H), 2.76 (d, *J* = 4.4 Hz, 3H). <sup>13</sup>C NMR (100 MHz, DMSO-*d*<sub>6</sub>) δ 166.80, 160.94, 160.01, 157.97, 156.17, 142.76, 139.80, 129.63, 128.25, 127.95,

126.49, 123.81, 118.85, 118.32, 111.81, 111.55, 99.02, 55.66, 26.70. HRMS (ESI) calcd for C<sub>20</sub>H<sub>18</sub>F<sub>3</sub>N<sub>6</sub>O<sub>2</sub> [M – H]<sup>–</sup>: 416.1334; found: 416.1327. R<sub>T,HPLC</sub> = 12.99 min, purity >99%.

4.2.22. 4-((4-((4-methoxyphenyl)amino)-5-(trifluoromethyl)pyrimidin-2-yl)amino)-N-methylbenzamide (**12h**)

White solid; 57% yield; m. p. 251.4–255.0 °C; <sup>1</sup>H NMR (400 MHz, CD<sub>3</sub>OD) δ 8.23 (s, 1H), 7.56–7.50 (s, 4H), 7.30 (d, *J* = 8.8 Hz, 2H), 6.97 (d, *J* = 8.8 Hz, 2H), 3.84 (s, 3H), 2.86 (s, 3H). <sup>13</sup>C NMR (100 MHz, CD<sub>3</sub>OD) δ 169.09, 160.61, 158.00, 154.89, 154.84, 142.94, 130.71, 127.61, 127.52, 127.44, 127.16, 126.15, 123.48, 118.38, 113.78, 113.75, 54.71, 25.52. HRMS (ESI) calcd for C<sub>20</sub>H<sub>18</sub>F<sub>3</sub>N<sub>6</sub>O<sub>2</sub> [M+H]<sup>+</sup>: 418.1485; found: 418.1482. R<sub>T,HPLC</sub> = 6.37 min, purity >96%.

4.2.23. 4-((3-((3-fluoro-4-methoxyphenyl)amino)-4-(trifluoromethyl)phenyl)amino)-N-methylbenzamide (**12i**)

White solid; 48% yield; m. p. 234.2–237.0 °C; <sup>1</sup>H NMR (400 MHz, CDCl<sub>3</sub>) δ 8.31 (s, 1H), 7.64 (d, *J* = 8.0 Hz, 2H), 7.54–7.52 (m, 3H), 7.45 (d, *J* = 12.0 Hz, 1H), 7.02 (d, *J* = 8.4 Hz, 1H), 6.96 (t, *J* = 8.8 Hz, 1H), 6.82 (s, 1H), 6.09 (s, 1H), 3.93 (s, 3H), 2.99 (d, *J* = 4.4 Hz, 3H). <sup>13</sup>C NMR (100 MHz, CDCl<sub>3</sub>) δ 167.72, 160.35, 157.66, 153.17, 150.73, 145.62, 145.51, 141.44, 130.20, 130.10, 129.06, 127.85, 119.23, 113.33, 113.30, 56.64, 26.95. HRMS (ESI) calcd for C<sub>20</sub>H<sub>17</sub>F<sub>4</sub>N<sub>5</sub>O<sub>2</sub> [M+H]<sup>+</sup>: 436.1391; found: 436.1393. R<sub>T,HPLC</sub> = 6.37 min, purity >96%.

4.2.24. 4-((4-((3-chloro-4-methoxyphenyl)amino)-5-(trifluoromethyl)pyrimidin-2-yl)amino)-N-methylbenzamide (**12j**)

White solid; 57% yield; m. p. 230.2–232.5 °C; <sup>1</sup>H NMR (400 MHz, DMSO-*d*<sub>6</sub>) δ 9.93 (s, 1H), 8.83 (s, 1H), 8.39 (s, 1H), 8.22 (q, *J* = 4.4 Hz, 1H), 7.6–7.57 (m, 4H), 7.54 (d, *J* = 2.8 Hz, 1H), 7.39 (dd, *J* = 8.8, 2.4 Hz, 1H), 7.19 (d, *J* = 8.8 Hz, 1H), 3.928 (s, 3H), 2.75 (d, *J* = 4.4 Hz, 1H). <sup>13</sup>C NMR (100 MHz, DMSO-*d*<sub>6</sub>) δ 166.77, 160.89, 158.12, 156.18, 156.13, 152.76, 142.76, 131.87, 128.24, 128.12, 128.03, 126.70, 120.90, 118.72, 112.83, 56.84, 26.69. HRMS (ESI) calcd for C<sub>20</sub>H<sub>17</sub>ClF<sub>3</sub>N<sub>5</sub>O<sub>2</sub> [M+H]<sup>+</sup>: 452.1095; found: 452.1084. R<sub>T,HPLC</sub> = 6.37 min, purity >95%.

4.2.25. 4-((4-((4-acetamidophenyl)amino)-5-(trifluoromethyl)pyrimidin-2-yl)amino)-N-methylbenzamide (**12k**)

White solid; 46% yield; m. p. 278.2–279.5 °C; <sup>1</sup>H NMR (400 MHz, DMSO-*d*<sub>6</sub>) δ 10.10 (s, 1H), 9.91 (s, 1H), 8.82 (s, 1H), 8.38 (s, 1H), 8.18 (d, *J* = 4.4 Hz, 1H), 7.63–7.60 (m, 6H), 7.38 (d, *J* = 8.8 Hz, 2H), 2.76 (d, *J* = 4.4 Hz, 3H), 2.10 (s, 3H). <sup>13</sup>C NMR (100 MHz, DMSO-*d*<sub>6</sub>) δ 168.97, 166.78, 166.76, 160.88, 142.87, 137.21, 133.56, 127.97, 127.92, 119.72, 118.66, 100.00, 26.70, 24.55. HRMS (ESI) calcd for C<sub>21</sub>H<sub>19</sub>F<sub>3</sub>N<sub>6</sub>O<sub>2</sub> [M+H]<sup>+</sup>: 444.1590; found: 444.1589. R<sub>T,HPLC</sub> = 11.39 min, purity >98%.

4.2.26. N-methyl-4-((4-((4-((methylsulfinyl)amino)phenyl)amino)-5-(trifluoromethyl)pyrimidin-2-yl)amino)benzamide (**12l**)

White solid; 40% yield; m. p. 282.5–284.6 °C; <sup>1</sup>H NMR (400 MHz, DMSO-*d*<sub>6</sub>) δ 9.93 (s, 1H), 9.86 (s, 1H), 8.86 (s, 1H), 8.40 (s, 1H), 8.16 (d, *J* = 4.4 Hz, 1H), 7.59 (s, 4H), 7.43 (d, *J* = 8.4 Hz, 2H), 7.27 (d, *J* = 8.8 Hz, 2H), 3.04 (s, 3H), 2.76 (d, *J* = 4.4 Hz, 3H). <sup>13</sup>C NMR (100 MHz, DMSO-*d*<sub>6</sub>) δ 172.49, 170.87, 166.94, 160.89, 158.11, 156.03, 142.76, 136.04, 134.80, 128.24, 127.90, 127.43, 126.49, 120.83, 120.77, 118.94, 60.27, 26.69. HRMS (ESI) calcd for C<sub>20</sub>H<sub>19</sub>F<sub>3</sub>N<sub>6</sub>O<sub>2</sub>S [M – H]<sup>–</sup>: 479.1113; found: 479.1066. R<sub>T,HPLC</sub> = 11.76 min, purity >99%.

### 4.3. Biochemistry

#### 4.3.1. Kinase assay

*In vitro* FAK, VEGFR2, PYK2, TRKA, TRKB, TRKC, JAK2, JAK3, and TYK2 kinases inhibition potency were measured using radiometric assay provided by Kinase Profiler service (ICE Bioscience Co. Ltd,

China). The synthesized compounds were diluted step-by-step from a concentrated stock of 8  $\mu\text{M}$  in 100% DMSO and with serial kinase reaction buffer dilutions. Taking FAK as an example, FAK was incubated with the title compounds in 25  $\mu\text{L}$  reaction solutions, and the reaction was initiated by adding the Mg-ATP mix. After incubation for 40 min at room temperature, the reaction was stopped by the addition of phosphoric acid to a concentration of 0.5%. 10  $\mu\text{L}$  of the reaction was then spotted onto a P30 filtermat and washed four times for 4 min in 0.425% phosphoric acid and once in methanol prior to drying and scintillation counting.

#### 4.3.2. Cell lines and culture conditions

Human pancreatic cancer cells PANC-1, human breast cancer cells MDA-MB-231, human umbilical vein endothelial cells HUVECs, human lung cancer cell A549, human normal embryonic kidney cells HEK293, and human hepatic cell line L02 were cultured in DMEM medium (high glucose). Human pancreatic cancer cells BxPC-3 and human colon cancer cell lines HCT-15 were cultured in RPMI-1640. Human liver cancer cells HepG2 and human breast cancer cells MCF-7 were cultured in MEM medium. All the mediums were supplemented with 10% FBS (HyClone, GE Healthcare, Australia) and 1% ampicillin/streptomycin, and incubated at 37 °C in a humidified atmosphere (5% CO<sub>2</sub> and 95% air).

#### 4.3.3. MTT assay

The title compounds were tested their anti-proliferative activities through MTT analysis on different cells. Defactinib was used as positive control. Cells were seeded in 96-well plates at a density of 2000 to 5000 cells/well. At the end of 24 h, the cells were treated with test compounds and incubated at 37 °C for 72 h. 3-(4,5-dimethylthiazol-2-yl)-2,5-diphenyltetrazolium bromide (MTT) was added to each well with final concentration of 0.5 mg/mL and incubated for 4 h. Then the medium was decanted and 150  $\mu\text{L}$  of DMSO was added to each well. The absorbance was obtained by a microplate reader (B20-TEK ELX800UV, USA) at 570 nm and all the measurements were conducted for three times under the same condition. IC<sub>50</sub> values were calculated by Graphpad Prism 5.

#### 4.3.4. Colony formation assay

Cancer cells were seeded in 6-well culture clusters overnight at 37 °C in 5% CO<sub>2</sub>, and treated with various concentrations of **11b** and **12f** (0.125, 0.25, 0.5, 1, 2  $\mu\text{M}$ ) for 10 d. Then, the medium was removed and the cells were washed with cold PBS, fixed with 4% paraformaldehyde and stained with a 1% crystal violet solution for 20 min. The colonies (>50 cells) were photographed and quantified by ImageJ software.

#### 4.3.5. Cell scratch assay

Cell migration inhibitory effects of compounds **11b** and **12f** were determined by scratch assay. PANC-1 cells or HUVECs were cultured in 6-well culture plates until the concentration reached 80–90%. Then, a cell free line was manually created by scratching the confluent cell monolayers with a 0.1 mL sterile pipette tips, and non-adherent cells were washed out by PBS. Fresh medium containing 10% FBS and different concentrations of test compounds (0.5, 1, 2, 4, 8  $\mu\text{M}$ ) was added. After 24 h, the images were captured by a microscope (Nikon ECLIPSE TE2000-U, Japan). Each experiment was conducted at least triplicate.

#### 4.3.6. Invasion assay

Cell motility inhibitory effects of compounds **11b** and **12f** were also examined using transwell assay on PANC-1 cells. Briefly, cells were harvested and resuspended in serum-free medium that containing 1, 2, 4  $\mu\text{M}$  of **11b** and **12f**, and added into the upper wells of transwell chamber (Millicell, 8  $\mu\text{m}$  pore size, 12-mm diameter,

Millipore) at a density of  $2 \times 10^5$  cells/mL. While DMEM containing 10% FBS was added into the lower chambers coated with 50  $\mu\text{L}$  of Matrigel (1:3 dilution in serum-free medium, Corning/BD Biosciences). After 20 h of incubation, the invasion cells were fixed with 4% paraformaldehyde and stained with 0.2% crystal violet for 30 min. Then, the chambers were washed with PBS and left to dry. Cells migrated to lower chamber were photographed using a digital camera with inverted microscope (Nikon ECLIPSE TE2000-U, Japan), and the cells were counted randomly in three independent fields.

#### 4.3.7. Apoptotic assay with PI/Hoechst 33258 staining method

PANC-1 ( $2 \times 10^4$ ) were cultured in 6-well plates at 37 °C in 5% CO<sub>2</sub> for 24 h. The cells were then incubated with medium containing different concentrations of **11b** and **12f** (0.1, 0.5, 2.5  $\mu\text{M}$  for PI staining; 0.25, 0.5, 1, 2, 4  $\mu\text{M}$  for Hoechst 33258 staining) for 48 h. Subsequently, removing the medium and washing cells with PBS, the cells were fixed with 4% paraformaldehyde for 30 min at room temperature, resuspended in 200  $\mu\text{L}$  PI staining buffer (10 mg/mL, Sigma, St. Louis, MO, USA) or staining buffer Hoechst 33258 (10 mg/mL, Sigma, St. Louis, MO, USA), and incubated in the dark at room temperature for 10 min. Afterwards, the cells were observed and imaged with a fluorescence microscope (Nikon ECLIPSE TE2000-U, Japan).

#### 4.3.8. Live/dead cell analysis

PANC-1 cells ( $2 \times 10^4$ ) were cultured in 6-well plates at 37 °C in 5% CO<sub>2</sub> for 24 h. The cells were washed with PBS and incubated with medium containing 0.25, 0.5, 1, 2, and 4  $\mu\text{M}$  of **11b** and **12f** for 48 h. Then, removing the medium and washing cells with PBS, the cells were resuspended in the solution containing 100  $\mu\text{L}$  FDA (0.02 mg/mL, Sigma, St. Louis, MO, USA) and 30  $\mu\text{L}$  PI (0.02 mg/mL, Sigma, St. Louis, MO, USA), and incubated in the dark at room temperature for 10 min. Afterwards, the cells were observed and imaged with a fluorescence microscope.

#### 4.3.9. F-actin phalloidin staining

The effects of compounds **11b** and **12f** on the morphology of PANC-1 cells were analyzed by F-actin staining. Briefly, the cells were seeded in 6-well plates with a glass bottom overnight at 37 °C, and were treated with 0, 0.25, 1, 2, 4, 8  $\mu\text{M}$  of **11b** and **12f** for 24 h. Media was then removed, and the cells were fixed in 4% paraformaldehyde for 5 min and washed thrice with PBS. A solution (200  $\mu\text{L}$ ) of 100 nM in MeOH FITC-phalloidin (Molecular Probes, Eugene, OR) containing 1% BSA was added and incubated for 30 min in darkness. Subsequently, the cells were washed thrice with PBS and stained with 200  $\mu\text{L}$  of DAPI (10  $\mu\text{g}/\text{mL}$ , Solarbio Science & Technology, China) for 5 min at 37 °C. Images were acquired using Nikon ECLIPSE TE2000-U inverted epifluorescent microscope using appropriate filters.

#### 4.3.10. Cell apoptosis assay

The apoptosis of PANC-1 cells was evaluated through flow cytometric analysis using a FACScan flow cytometer (BECKMAN Cytomics™ FC 500, USA). PANC-1 cells were seeded in 6-well plates overnight at 37 °C, and 0.2, 1, 5  $\mu\text{M}$  of **11b** or **12f** were added in triplicate for 48 h incubation. Suspension cells were centrifuged at 2000 rpm for 5 min, and adherent cells were digested with trypsin without EDTA and washed with PBS twice. Then all the cells were resuspended in 500  $\mu\text{L}$  binding buffer, and 5  $\mu\text{L}$  Annexin V-FITC and 5  $\mu\text{L}$  PI (Keygen Biotech, China) working solution were successively added in 500  $\mu\text{L}$  cell suspension and incubated for 15 min and 5 min in total dark, respectively. Subsequently, flow cytometry was performed using a FACScan flow cytometry. Data were analyzed by FlowJo 10 software.

#### 4.3.11. Cell cycle analysis

PANC-1 cells were seeded in 6-well plates overnight at 37 °C, and 0.2, 1, 5 μM of **11b**, and **12f** were added in triplicate for 24 h incubation. Then cells were harvested, washed twice with cold PBS, and then fixed with ethanol (70%) at 4 °C overnight. The cells were centrifuged to remove the fixative solution and washed twice with cold PBS. Subsequently, the cells were stained with 500 μL PI/RNase working solution (Keygen Biotech, China) at 4 °C for 30 min in the dark. The cells were analyzed using a flow cytometer.

#### 4.3.12. Western blotting method to analyze apoptosis-related proteins

The protein levels in PANC-1 cells were assessed via Western blot analysis. Cells were seeded into cell culture dishes (1 × 10<sup>7</sup> cells per dish) and incubated overnight at 37 °C, and 0.25, 0.5, 1, 2, 4 μM of **11b**, and **12f** were added in triplicate for 24 h incubation. Cells were then harvested and lysed in Laemmli buffer (glycerol, 1 M TRIS pH 6.8, 1% SDS, mQH<sub>2</sub>O and 20% β-mercaptoethanol) with bromophenol blue. Samples were boiled for 5 min at 95 °C and kept at −80 °C until usage. The protein content was determined by a BCA kit. Equal amounts of 30 μg per lane of protein were placed on a Tris/HCl gel, and the protein was separated by SDS-PAGE electrophoresis. After the electrophoresis, the samples were transferred to PVDF (Milibo, Co. Ltd., USA) membrane and blocked with 5% skimmed milk powder for 2 h. Diluted primary antibodies FAK (1 : 1000), p-FAK (1 : 1000), PI3K (1 : 2000), p-PI3K (1 : 1000), AKT (1 : 1000), p-AKT (1 : 1000), cyclin D1 (1 : 1000), Bcl-2 (1 : 3000), Bax (1 : 10000), and GAPDH (1 : 10000) were incubated overnight at 4 °C followed by a horseradish peroxidase-labeled goat anti-rabbit IgG secondary antibody (ProteinTech, China) for 2 h at room temperature. Immunoreactivity was developed with diaminobenzidine solution, and scanned and recorded by a gel imaging system (G:BDX Chemi XL1.4, Genome Co., Ltd.).

#### 4.3.13. Kinase-inhibition assays

The potential of **12f** as a kinase inhibitor was determined at the concentration of 1 μmol/L against a panel of 74 tyrosine kinases through the commercially available service provided by ICE bioscience (ICE Bioscience Co. Ltd, China).

#### 4.3.14. Tube formation assay

Briefly, a 96-microwell plate pre-chilled at 4 °C was carefully filled with 50 μL/well of liquid Matrigel (10 mg/mL, Corning, USA) at 4 °C with a pre-chilled pipette, avoiding bubbles. The Matrigel was polymerized for 1 h at 37 °C, and 100 μL HUVECs suspension (2 × 10<sup>4</sup>) were added to each well. Subsequently, the cells were cultured with 1, 2, 4 μM of **11b** and **12f** for 8 h. The tube formation was observed and counted with an inverted microscope.

#### 4.3.15. Zebrafish embryo assay

Transgenic *fli-1*: enhanced GFP zebrafish embryos were generated by natural pairwise mating and raised at 28 °C in embryo water (60 mmol/L NaCl, 2.4 mmol/L sodium bicarbonate, 0.8 mmol/L CaCl<sub>2</sub>, 0.67 mmol/L KCl, and 10 mmol/L HEPES). 6 h post fertilization (hpf), the dead and unhealthy embryos were removed, and the embryos were sorted in the 24-well plate (twenty embryos/well). Then the embryos were treated with 0.5, 1, 2 μM of **11b** and **12f** for 24 h at 28.5 °C. Subsequently, the embryos were anesthetized with 0.01% tricaine in embryo water and photographed.

#### Declaration of competing interest

The authors declare that they have no known competing financial interests or personal relationships that could have appeared to influence the work reported in this paper.

#### Acknowledgments

This work was supported by the National Natural Science Foundation of China (81660570, U1812403), Guizhou Medical University 2018 Academic New Seedling Training and Innovation Exploration Project ([2017]5718, [2018]5779-13, [2018]5779-75), Key Research Project of Science and Technology Department of Guizhou Province (Qiankehejichu [2020]1Z008, [2020]1Z068), Special Foundation of the Central Government to Guide Local Science and Technology ([2019]4008), and Guizhou Science and Technology Department (Nos. 2020-5006 and 2020-6011).

#### Appendix A. Supplementary data

Supplementary data to this article can be found online at <https://doi.org/10.1016/j.ejmech.2021.113573>.

#### References

- [1] V.M. Golubovskaya, F.A. Kweh, W.G. Cance, Focal adhesion kinase and cancer, *Histol. Histopathol.* 24 (2009) 503–510.
- [2] B.Y. Lee, P. Timpson, L.G. Horvath, R.J. Daly, FAK signaling in human cancer as a target for therapeutics, *Pharmacol. Ther.* 146 (2015) 132–149.
- [3] H. Yoon, J.P. Dehart, J.M. Murphy, S.T.S. Lim, Understanding the roles of FAK in cancer: inhibitors, genetic models, and new insights, *J. Histochem. Cytochem.* 63 (2015) 114–128.
- [4] L. Tremblay, W. Hauck, A.G. Aprikian, L.R. Begin, A. Chapdelaine, S. Chevalier, Focal adhesion kinase (pp125FAK) expression, activation and association with paxillin and p50CSK in human metastatic prostate carcinoma, *Int. J. Canc.* 68 (1996) 164–171.
- [5] P.L. Judson, X. He, W.G. Cance, L.V. Le, Overexpression of focal adhesion kinase, a protein tyrosine kinase, in ovarian carcinoma, *Cancer* 86 (1999) 1551–1556.
- [6] T. Lechertier, K. Hovidala-Dilke, Focal adhesion kinase and tumour angiogenesis, *J. Pathol.* 226 (2011) 404–412.
- [7] S.J. McCormack, S.E. Brazinski, J.L. Moore Jr., B.A. Werness, D.J. Goldstein, Activation of the focal adhesion kinase signal transduction pathway in cervical carcinoma cell lines and human genital epithelial cells immortalized with human papillomavirus type 18, *Oncogene* 15 (1997) 265–274.
- [8] J. Zhang, S.N. Hochwald, The role of FAK in tumor metabolism and therapy, *Pharmacol. Ther.* 142 (2014) 154–163.
- [9] V.M. Golubovskaya, C. Virnig, W.G. Cance, TAE226-induced apoptosis in breast cancer cells with overexpressed Src or EGFR, *Mol. Carcinog.* 47 (2010) 222–234.
- [10] E. Shanthi, M.H. Krishna, G.M. Arunesh, K.V. Reddy, J.S. Kumar, V.N. Viswanadhan, Focal adhesion kinase inhibitors in the treatment of metastatic cancer: a patent review, *Expert Opin. Ther. Pat.* 24 (2014) 1077–1100.
- [11] S.F. Jones, L.L. Siu, J.C. Bendell, J.M. Cleary, A.R.A. Razak, J.R. Infante, S.S. Pandya, P.L. Bedard, K.J. Pierce, B. Houk, A phase I study of VS-6063, a second-generation focal adhesion kinase inhibitor, in patients with advanced solid tumors, *Invest. N. Drugs* 33 (2015) 1100–1107.
- [12] G.R. Ott, M. Cheng, K.S. Learn, J. Wagner, D.E. Gingrich, J.G. Lisko, M. Curry, E.F. Mesaros, A.K. Ghose, M.R. Quail, Discovery of clinical candidate CEP-37440, a selective inhibitor of focal adhesion kinase (FAK) and anaplastic lymphoma kinase (ALK), *J. Med. Chem.* 59 (2016) 7478–7496.
- [13] I. Tanjoni, C. Walsh, S. Uryu, A. Tomar, J.O. Nam, A. Mielgo, S.T. Lim, C. Liang, M. Koenig, C. Sun, N. Patel, C. Kwok, G. McMahon, D.G. Stupack, D.D. Schlaepfer, PND-1186 FAK inhibitor selectively promotes tumor cell apoptosis in three-dimensional environments, *Canc. Biol. Ther.* 9 (2010) 764–777.
- [14] C. Walsh, I. Tanjoni, S. Uryu, A. Tomar, J.O. Nam, H. Luo, A. Phillips, N. Patel, C. Kwok, G. McMahon, D.G. Stupack, D.D. Schlaepfer, Oral delivery of PND-1186 FAK inhibitor decreases tumor growth and spontaneous breast to lung metastasis in pre-clinical models, *Canc. Biol. Ther.* 9 (2010) 778–790.
- [15] T. Heinrich, J. Seenisamy, L. Emmanuvel, S.S. Kulkarni, J. Bomke, F. Rohdich, H. Greiner, C. Esdar, M. Krier, U. Grädler, D. Musil, Fragment-based discovery of new highly substituted 1H-pyrrolo[2,3-b]- and 3H-imidazo[4,5-b]-pyridines as focal adhesion kinase inhibitors, *J. Med. Chem.* 56 (2013) 1160–1170.
- [16] M. Iwatani, H. Iwata, A. Okabe, R.J. Skene, N. Tomita, Y. Hayashi, Y. Aramaki, D.J. Hosfield, A. Hori, A. Baba, H. Milki, Discovery and characterization of novel allosteric FAK inhibitors, *Eur. J. Med. Chem.* 61 (2013) 49–60.
- [17] G. Hallur, N. Tamizharasan, S.P. Sulochana, N.K. Saini, M. Zainuddin, R. Mullangi, LC-ESI-MS/MS determination of defactinib, a novel FAK inhibitor in mice plasma and its application to a pharmacokinetic study in mice, *J. Pharmaceut. Biomed. Anal.* 149 (2018) 358–364.
- [18] M. Ai, C. Wang, Z. Tang, K. Liu, X. Sun, T. Ma, Y. Li, X. Ma, L. Li, L. Chen, Design and synthesis of diphenylpyrimidine derivatives (DPPYs) as potential dual EGFR T790M and FAK inhibitors against a diverse range of cancer cell lines, *Bioorg. Chem.* 94 (2020) 103408.

- [19] A.O. Walter, R.T. Sjin, H.J. Haringsma, K. Ohashi, J. Sun, K. Lee, A. Dubrovskiy, M. Labenski, Z. Zhu, Z. Wang, M. Sheets, T. St Martin, R. Karp, D. van Kalken, P. Chaturvedi, D. Niu, M. Nacht, R.C. Petter, W. Westlin, K. Lin, S. Jaw-Tsai, M. Raponi, T. Van Dyke, J. Etter, Z. Weaver, W. Pao, J. Singh, A.D. Simmons, T.C. Harding, A. Allen, Discovery of a mutant-selective covalent inhibitor of EGFR that overcomes T790M-mediated resistance in NSCLC, *Canc. Discov.* 3 (2013) 1404–1415.
- [20] Z. Song, S. Huang, H. Yu, Y. Jiang, C. Wang, Q. Meng, X. Shu, H. Sun, K. Liu, Y. Li, X. Ma, Synthesis and biological evaluation of morpholine-substituted diphenylpyrimidine derivatives (Mor-DPPYs) as potent EGFR T790M inhibitors with improved activity toward the gefitinib-resistant non-small cell lung cancers (NSCLC), *Eur. J. Med. Chem.* 133 (2017) 329–339.
- [21] P. Dao, D. Lietha, M. Etheve-Quelquejeu, C. Garbay, H. Chen, Synthesis of novel 1,2,4-triazine scaffold as FAK inhibitors with antitumor activity, *Bioorg. Med. Chem. Lett* 27 (2017) 1727–1730.
- [22] R. Wang, S. Yu, X. Zhao, Y. Chen, B. Yang, T. Wu, C. Hao, D. Zhao, M. Cheng, Design, synthesis, biological evaluation and molecular docking study of novel thieno[3,2-d]pyrimidine derivatives as potent FAK inhibitors, *Eur. J. Med. Chem.* 188 (2020) 112024.
- [23] B.-T. Berger, M. Amaral, D.B. Kokh, A. Nunes-Alves, D. Musil, T. Heinrich, M. Schröder, R. Neil, J. Wang, I. Navratilova, J. Bomke, J.M. Elkins, S. Müller, M. Frech, R.C. Wade, S. Knapp, Structure-kinetic relationship reveals the mechanism of selectivity of FAK inhibitors over PYK2, *Cell Chem. Biol.* 28 (2021) 686–698.
- [24] T. Shimizu, K. Fukuoka, M. Takeda, T. Iwasa, T. Yoshida, J. Horobin, M. Keegan, L. Vaickus, A. Chavan, M. Padval, K. Nakagawa, A first-in-Asian phase 1 study to evaluate safety, pharmacokinetics and clinical activity of VS-6063, a focal adhesion kinase (FAK) inhibitor in Japanese patients with advanced solid tumors, *Canc. Chemother. Pharmacol.* 77 (2016) 997–1003.
- [25] J. Zhang, B. Wang, Arsenic trioxide (As<sub>2</sub>O<sub>3</sub>) inhibits peritoneal invasion of ovarian carcinoma cells in vitro and in vivo, *Gynecol. Oncol.* 103 (2006) 199–206.
- [26] P. Gunning, G. O'Neill, E. Hardeman, Tropomyosin-based regulation of the actin cytoskeleton in time and space, *Physiol. Rev.* 88 (2008) 1–35.
- [27] Y.J. Choi, J.M. Hur, S. Lim, M. Jo, D.H. Kim, J.I. Choi, Induction of apoptosis by deinoxanthin in human cancer cells, *Anticancer Res.* 34 (2014) 1829–1835.
- [28] Y. Liu, C. Liu, T. Tan, S. Li, S. Tang, X. Chen, Sinomenine sensitizes human gastric cancer cells to cisplatin through negative regulation of PI3K/AKT/Wnt signaling pathway, *Anti Canc. Drugs* 30 (2019) 983–990.
- [29] V. Thamilselvan, D.H. Craig, M.D. Basson, FAK association with multiple signal proteins mediates pressure-induced colon cancer cell adhesion via a Src-dependent PI3K/Akt pathway, *Faseb. J.* 21 (2007) 1730–1741.
- [30] S. Reif, A. Lang, J.N. Lindquist, Y. Yata, E. Gabele, A. Scanga, D.A. Brenner, R.A. Rippe, The role of focal adhesion kinase-phosphatidylinositol 3-kinase-akt signaling in hepatic stellate cell proliferation and type I collagen expression, *J. Biol. Chem.* 278 (2003) 8083–8090.
- [31] F.J. Sulzmaier, C. Jean, D.D. Schlaepfer, FAK in cancer: mechanistic findings and clinical applications, *Nat. Rev. Canc.* 14 (2014) 598–610.
- [32] Y. Zhang, M. Moschetta, D. Huynh, Y.-T. Tai, Y. Zhang, W. Zhang, Y. Mishima, J.E. Ring, W.F. Tam, Q. Xu, P. Maiso, M. Reagan, I. Sahin, A. Sacco, S. Manier, Y. Aljawai, S. Glavey, N.C. Munshi, K.C. Anderson, J. Pachter, A.M. Roccaro, I.M. Ghobrial, Pyk2 promotes tumor progression in multiple myeloma, *Blood* 124 (2014) 2675–2686.
- [33] A.M. Lange, H.-W. Lo, Inhibiting TRK proteins in clinical cancer therapy, *Cancers* 10 (2018) 105.
- [34] A. Hosseini, T. Gharibi, F. Marofi, M. Javadian, Z. Babaloo, B. Baradaran, Janus kinase inhibitors: a therapeutic strategy for cancer and autoimmune diseases, *J. Cell. Physiol.* 235 (2020) 5903–5924.
- [35] K. Wöss, N. Simonović, B. Strobl, S. Macho-Maschler, M. Müller, TYK2: an upstream kinase of STATs in cancer, *Cancers* 11 (2019) 1728.
- [36] K.J. Png, N. Halberg, M. Yoshida, S.F. Tavazoie, A microRNA regulon that mediates endothelial recruitment and metastasis by cancer cells, *Nature* 481 (2011) 190–194.
- [37] H.J. Park, Y. Zhang, S.P. Georgescu, K.L. Johnson, D. Kong, J.B. Galper, Human umbilical vein endothelial cells and human dermal microvascular endothelial cells offer new insights into the relationship between lipid metabolism and angiogenesis, *Stem Cell Rev.* 2 (2006) 93–102.
- [38] H. Fan, D. Wei, K. Zheng, X. Qin, L. Yang, Y. Yang, Y. Duan, Y. Xu, L. Hu, Discovery of Dioxino[2,3-f]quinazoline derivative VEGFR-2 inhibitors exerting significant antiproliferative activity in HUVECs and mice, *Eur. J. Med. Chem.* 175 (2019) 349–356.
- [39] S. Soeda, T. Kozako, K. Iwata, H. Shimeno, Oversulfated fucoidan inhibits the basic fibroblast growth factor-induced tube formation by human umbilical vein endothelial cells: its possible mechanism of action, *Biochim. Biophys. Acta* 1497 (2000) 127–134.
- [40] J. Rocke, J. Lees, I. Packham, T. Chico, The zebrafish as a novel tool for cardiovascular drug discovery, *Recent Pat. Cardiovasc. Drug Discov.* 4 (2009) 1–5.